Electron-Positron Interactions at High Energies

B. Bartoli, F. Felicetti, H. Ogren, and V. Silvestrini
Laboratori Nazionali di Frascati del Comitato Nazionale per l'Energia Nucleare, Frascati, Italy

and

G. Marini
Istituto di Fisica dell'Università di Roma e Sezione di Roma dell'Istituto Nazionale di Fisica Nucleare, Roma, Italy

and

A. Nigro and F. Vanoli
Istituto di Fisica dell'Università di Napoli e Sezione di Napoli dell'Istituto Nazionale di Fisica Nucleare, Napoli, Italy
(Received 9 May 1972)

The results of an experiment performed at Adone, the 2×1.5-GeV e^+e^- Frascati storage ring, are presented. During ~ 1500 hours of running time a total of 5164 electron-positron elastic scattering events (integrated luminosity $\mathcal{L}=3.5\times10^{35}$ cm^{-2}) and 605 noncoplanar events from the reaction $e^+e^-\to a^\pm+b^\pm+$ anything (effective integrated luminosity $\mathcal{L}=2.5\times10^{35}$ cm^{-2}) have been collected at c.m. energies ranging from 1.4 to 2.4 GeV. Over the energy range explored (1.4–2.4 GeV), corresponding to an average q^2 ranging from 0.8 to 2.4 (GeV/c)^2, the yield of wide-angle ($60°<\theta<120°$) electron-positron elastic scattering events is found to be in good agreement with the predictions of quantum electrodynamics (QED) ($R=\sigma_{\text{exp}}/\sigma_{\text{QED}}=1.05\pm0.04$). The noncoplanar events appear to be of a hadronic nature and are produced with a much higher cross section than predicted on the basis of ρ, ω, ϕ dominance at these energies. The total cross section for the reaction $e^+e^-\to a^\pm b^\pm+$ anything shows a rapid increase to ~ 90 nb between 1.0 and 1.5 GeV and falls off slowly to ~ 50 nb at 2.4 GeV. Cross sections for some of the channels contributing to this multihadron process ($e^+e^-\to\pi^+\pi^-\pi^+\pi^-$, $e^+e^-\to\pi^+\pi^-\pi^+\pi^-+$neutrals, $e^+e^-\to3\pi^+3\pi^-$) have been determined and are reported.

I. INTRODUCTION

We present here the final results of an experiment performed at Adone, the Frascati 2×1.5-GeV e^+e^- storage ring. The experiment was originally designed mainly to search for possible enhancements in the yield of particles produced in e^+e^- interactions which could indicate the existence of new vector bosons. Events due to e^+e^- wide-angle elastic scattering (Bhabha events) were collected at the same time, both as a test of quantum electrodynamics (QED) in the region of spacelike squared momentum transfers to the virtual photon up to 2.4 (GeV/c)^2 and as a monitor reaction for the hadronic channels.

When Adone came into operation, the electron-positron annihilation into hadrons, through the vector mesons ρ,ω,ϕ, had already been extensively studied at Orsay[1] and Novosibirsk.[2] As a crude extension of the ρ,ω,ϕ dominance model up to 2 GeV or more, the most popular tendency was to expect the production of hadrons to be very depressed at those relatively high energies.

It is now well known (see the preliminary results of this experiment published in 1970[3] and 1971[4] and confirmed by the results from other groups[5,6]) that the cross section for production of many hadrons in e^+e^- interactions turns out to be surprisingly larger than one would have expected.

These results have stimulated considerable theoretical activity.[7] Among the most attractive theories are the so-called pointlike models trying to relate these large values of the cross sections to the analogous well-known results on the spacelike channel obtained by the SLAC-MIT collaboration[8] studying the deep-inelastic scattering of electrons on protons. The problem of the interpretation of these storage-ring results is still quite open and much more work must be done both experimentally and theoretically in this field.

Concerning the results we are presenting in this paper, we would like to make a final remark. We are aware that even in this final version some features of our results are to a certain degree qualitative. In fact, our apparatus (as well as all the other first-generation apparatus operating at Adone) had not been designed in order to study the phenomenon which turned out to be the most important at the Adone energies, namely, the production of high-multiplicity final states. Nevertheless, we have thought it important to push the phenomenological interpretation as far as possible because multihadronic cross sections of this magnitude reveal an important new area of investigation

in the study of the structure of hadrons and of their electromagnetic currents.

II. THE EXPERIMENTAL APPARATUS

The experimental apparatus, shown in Fig. 1, surrounds one of the straight sections of Adone and covers about 0.35 of the total solid angle as seen from the center of the apparatus.[9]

Each of the four identical telescopes T_i consists of

(a) four plastic scintillation counters A_i, B_i, C_i, D_i;

(b) two magnetostrictive monogap wire spark chambers $SC\alpha_i$, $SC\beta_i$, which measure φ, the azimuthal direction of the final-state particles (z axis along the beam direction);

(c) the following absorbers: 1.3 cm Al between A_i and B_i; 0.7 cm Pb between B_i and C_i and between C_i and D_i. Signal pulses from the lead-scintillator-sandwich counter $(C_i + D_i)$ were used for pulse-height analysis to discriminate showering electrons from minimum-ionizing particles.

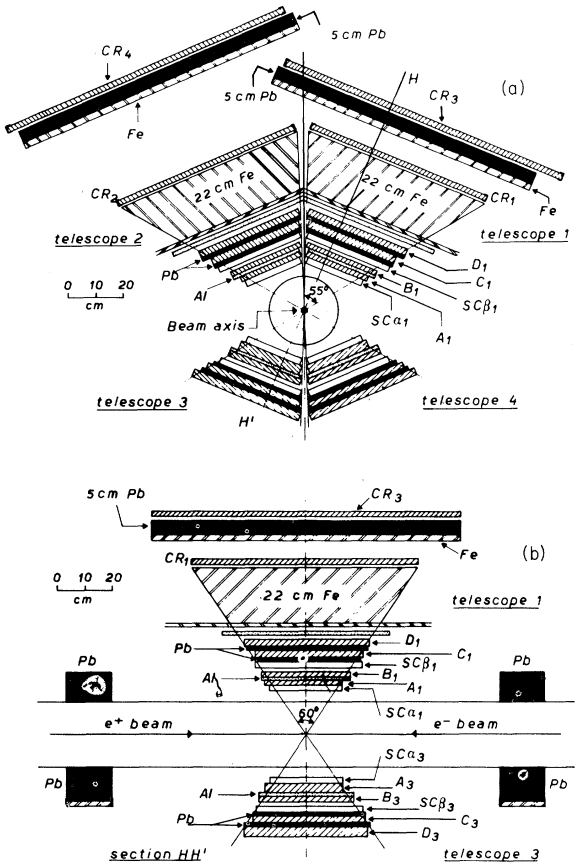

FIG. 1. The experimental apparatus. (a) Section orthogonal to the beam axis: A_i, B_i, C_i, D_i are plastic scintillator counters; $SC\alpha_i$ and $SC\beta_i$ are magnetostrictive monogap wire chambers; CR_i's are veto counters for cosmic rays. (b) Section (along H, H') in a plane through the beam direction and orthogonal to a pair of opposite telescopes.

These telescopes T_i cover the following angles, as measured from a coordinate system centered on the apparatus (z, along the e^+e^- direction; x, toward the center of the Adone ring):

$$T_1\ (60° < \theta < 120°,\ \ 28° < \varphi < 83°),$$

$$T_2\ (60° < \theta < 120°,\ \ 97° < \varphi < 152°),$$

$$T_3\ (60° < \theta < 120°,\ 208° < \varphi < 263°),$$

$$T_4\ (60° < \theta < 120°,\ 277° < \varphi < 332°).$$

A thick absorber (22 cm Fe) and a roof of veto counters CR_1 and CR_2 above the apparatus reduce the detected cosmic-ray flux by a factor $\gtrsim 100$. On the other hand the emitted particles we are interested in have only a relatively small probability of emerging from the Fe absorber and thus triggering the anticoincidence counters CR_1, CR_2; for the electrons this is due to the absorption of their electromagnetic showers, while for the hadrons this results from being stopped or nuclearly absorbed.

In a second set of measurements we have added a second roof, consisting of 1.5 cm of Fe and 5 cm of Pb, and two additional counters CR_3 and CR_4 (see Fig. 1). During this second set of measurements, CR_3 and CR_4 were used in anticoincidence, while CR_1, CR_2 were simply recorded in association with each event. From the number of the detected marked events (i.e., the events not vetoed by $CR_3 + CR_4$ but in which CR_1 or/and CR_2 were triggered) we were able to measure the anticoincidence corrections to be applied to the first set of data (i.e., with $CR_1 + CR_2$ in anticoincidence) and obtain as well direct information on the penetration of the detected particles.

A charged particle in telescope T_i is defined by the coincidence $\mathcal{T}_i \equiv A_i B_i (C_i + D_i)$. A neutral particle is then defined as $\mathcal{N}_i \equiv (\bar{A}_i + \bar{B}_i)(C_i + D_i)$. Any coincidence of two or more charged particles ($\mathcal{T}_i$), each in a different telescope, defines the master coincidence, the CR counters being set in anticoincidence ($CR = CR_1 + CR_2$ in the first set of measurements, while $CR = CR_3 + CR_4$ in the second set). To give a $\mathcal{T}_i$ coincidence a particle must thus traverse 24 g/cm^2 of absorber, corresponding to $\sim 1.9 X_0$ radiation lengths; to reach CR_1, CR_2 it must traverse $15 X_0 = 203$ g/cm^2; to be vetoed by CR_3, CR_4 it must traverse $25.2 X_0 = 282$ g/cm^2. Consequently, if the particle is a pion, it must have a minimum kinetic energy of ~75 MeV to be detected (i.e., to give a $\mathcal{T}_i$ coincidence). To be marked (or vetoed) by $CR_1 + CR_2$ the pion must have $\gtrsim 350$ MeV, while pions with more than ~500 MeV are vetoed by CR_3

and CR_4 unless they are absorbed by nuclear interactions (actually the fraction of particles absorbed is quite large, e.g., 85% of 400 MeV pions). On the other hand, practically all the electrons with less than 1.2 GeV are absorbed before being vetoed by CR_3, CR_4, while the fraction of the electrons able to trigger CR_1+CR_2 strongly depends on the energy, increasing from zero at $E_\pm \sim 500$ MeV up to ~15% at 1.2 GeV (see Sec. IV C).

When a master trigger occurs a PDP8 computer records the following:

(i) which coincidences $\mathcal{T}_i$ (or $\mathcal{H}_i$) were involved in the event;

(ii) the azimuthal coordinates (i.e., orthogonal to the beam direction) of the sparks in all the chambers $SC\alpha_i, SC\beta_i$ (with the restriction that when there is more than one track in the same chamber, only the closest one to the magnetostrictive pickup is detected[10]);

(iii) the pulse height H_i in the lead-scintillator sandwich (C_i+D_i) for each telescope T_i;

(iv) the time separation Δt between the occurrence of the event and a timing signal fixed to the zero crossing of the radio frequency (rf) accelerating voltage of the storage ring.[11]

All this information is recorded, event by event, on a magnetic tape for a later analysis on the 1108 Univac computer of the University of Rome.

During the running of the experiment, auxiliary information was accumulated with the PDP8 in a live display [e.g., histograms of uncorrelated pulse-height spectra from (C_i+D_i) for each telescope; the time distribution of the collected events; the distribution of the sparks in the various chambers, etc.] thus allowing a continuous check of the performance of the whole experimental apparatus.

III. DATA COLLECTION AND INITIAL REDUCTION

The results we present here had an effective total running time of ~1500 hours corresponding to a total integrated luminosity of the machine of $\mathcal{L} = \int L dt = 3.5\times10^{35}$ cm^{-2}.[12] The runs were performed at several values of the c.m. energy $E_+ + E_-$ ranging from 1.4 to 2.4 GeV.

In Table I for each c.m. energy the running time and the corresponding raw integrated luminosity are listed. We have also marked with an asterisk the measurements in which counters CR_3+CR_4 were set in anticoincidence (second set of measurements; see Sec. II). The other runs were instead performed with CR_1+CR_2 in anticoincidence (first set of measurements; see Sec. II). The quoted luminosities were evaluated by measuring with a monitor apparatus the yield of events from a process of known cross section, namely, e^+e^- scattering at small angles. This Bhabha-scattering monitor apparatus,[13] consisting of two symmetrical telescopes covering a range of c.m. angles, θ, between 3.5° and 6° (corresponding to four-momentum transfer to the virtual photon less than ~100 MeV/c), was operated by the $\mu\pi$ Group (see Ref. 5) in a contiguous straight section of Adone. The over-all uncertainty in the absolute normalization of the monitor is estimated to be ±5%. In addition by analyzing the relative variations of counting rates in the two symmetric telescopes we have evaluated as ±7% an additional time-dependent uncertainty mainly due to erratic changes in the position of the beams with respect to the monitor apparatus.[14]

TABLE I. Running times and integrated luminosities. The rows marked with an asterisk refer to runs in which counters CR_3+CR_4 were set in anticoincidence with the trigger (second set of measurements, see Sec. II).

c.m. energy $E_+ + E_-$ (GeV)	Running time (hours)	Integrated luminosity $\mathcal{L}$ (10^{32} cm^{-2})
1.40	85	68
1.40*	135	113
1.50	45	52
1.50*	163	280
1.60	62	77
1.65	77	114
1.70	84	126
1.75	96	135
1.80	76	135
1.85	119	260
1.85*	87	420
1.90	58	134
2.00	119	290
2.40	78	148
2.40*	221	1147
Totals	1505	3499

Over the total running period of this experiment we have collected a total of ~10^6 trigger events. The reasons for this high counting rate are the following. First, we have operated the master coincidence (between the telescopes T_i) with a very large resolving time τ ($\tau \simeq 40$ nsec). This allows us, on the basis of the analysis of the Δt distribution of the events, to very accurately define *a posteriori* the time interval in which the two bunches of e^+ and e^- collide, and also provides a very powerful way to evaluate the cosmic-ray contamination to the data. In fact [see Fig. 2(a)] a typical Δt distribution as it comes out from the computer shows a very clear peak [2 nsec, half width at half maximum (HWHM)] corresponding to the beam-beam impact, superimposed on a smooth background due to cosmic rays. Using these distributions we can define an interval of Δt for events in-time with the beam-beam interaction.

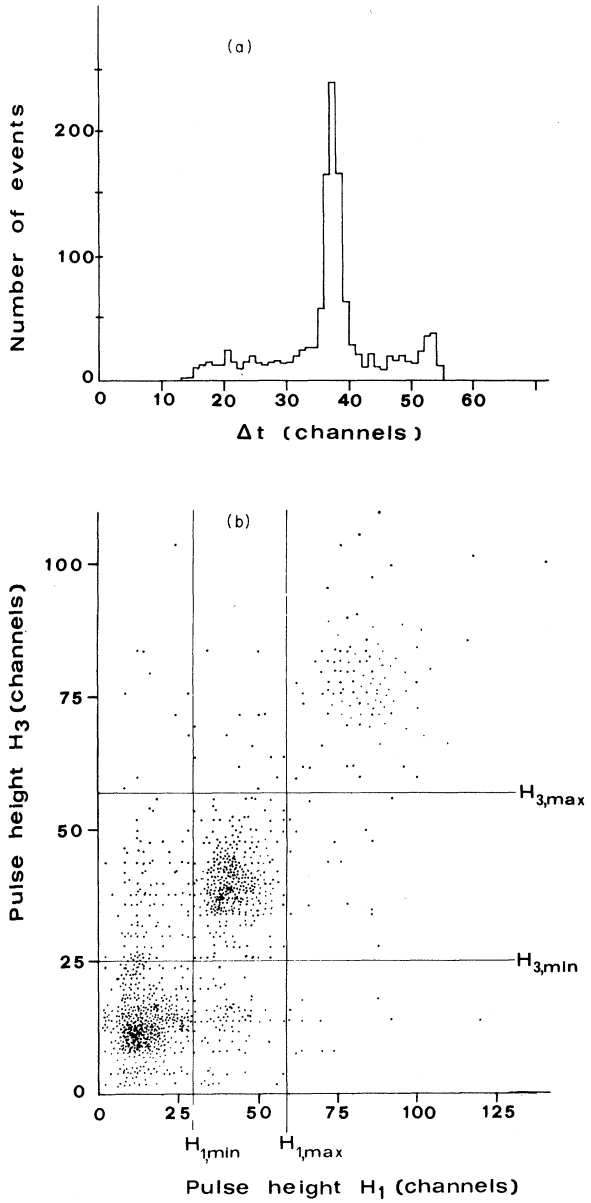

FIG. 2. Typical computer outputs for preliminary analysis. (a) Δt distribution of unselected events (Δt is the time separation between the occurrence of the event and a reference time fixed with the zero crossing of the *RF* accelerating voltage of the storage ring). (b) Pulse-height plot H_3 vs H_1 for (τ_1, τ_3) unselected events.

Secondly, the pulse-height thresholds of the discriminators were set much lower than the value corresponding to minimum-ionizing particles. Although this introduces in the trigger rates a great amount of machine background, it permits *a posteriori* a much more reliable separation of the minimum-ionizing particles from the background by allowing us to take into account any long-period drifts in the pulse-height spectrum. As an example, in Fig. 2(b) a typical plot of H_1 vs H_3 for the collected events is shown. A cluster corresponding to minimum-ionizing particles (mainly cosmic rays) is clearly visible and quite well separated from the low-pulse-height background. We can thus define for each telescope T_i two values, $H_{i,\min}$ $H_{i,\max}$, within which all the minimum-ionizing particles are confined.

The first steps of the analysis thus consist in selecting, run by run and energy by energy, all the events which occur in time with the beam-beam impact (in-time events), excluding in this way the majority of the cosmic-ray events (out-of-time events); and in rejecting the low-pulse-height machine background events by appropriately selecting the values for each telescope of the low-pulse-height cut $H_{i,\min}$.

The selection of the events we are interested in, and the identification of the particles, is made by observing the time occurrence of the event, the particle pulse heights, and the coplanarity angle between the tracks in different telescopes. In the next section we will discuss those events determined to be e^+e^- wide-angle elastic scattering. In Sec. V the multibody hadron events will be discussed.

IV. REACTION $e^+e^- \to e^+e^-$

A. Selection of the Events

The e^+e^- elastic scattering events are to be selected among the events which give a coincidence between opposite telescopes ($T_1 \cdot T_3$) and ($T_2 \cdot T_4$), and which occur in-time with the beam-beam interaction. As will be shown in this section, such a selection is possible in our apparatus simply on the basis of the pulse-height analysis in the sandwich counter ($C_i + D_i$) without the use of our experimental information on the geometry of each event.

Let us first examine the pulse-height distributions. Figure 3(a) shows a typical pulse-height plot of H_1 vs H_3 for ($T_1 \cdot T_3$) events which are in-time with the beam-beam impact. Two heavily populated regions are visible in the plot. The low-pulse-height region, confined between $H_{i,\min}$ and $H_{i,\max}$, contains the minimum-ionizing particles (mostly cosmic rays). The large-pulse-height region ($H_i \geq H_{i,\max}$, $i = 1, 3$) contains events with both the detected particles producing a detectable shower. We designate this large-pulse-height region as the $[e,e]$ region. The in-time events in this $[e,e]$ region ($[e,e]$ events) are good candidates to be $e^+e^- \to e^+e^-$ scattering events. The plot for out-of-time events, which turn out to be cos-

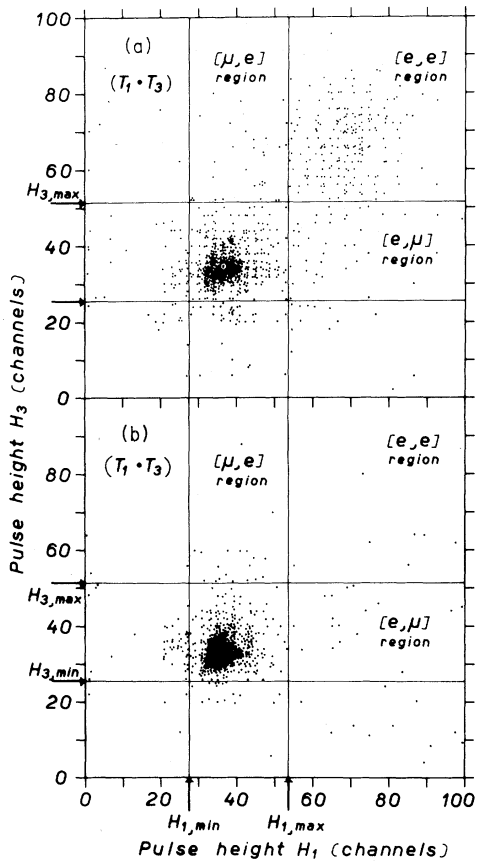

FIG. 3. Plot of pulse heights for $(T_1 \cdot T_3)$ events. (a) Events in-time with the beam-beam impact; (b) out-of-time events.

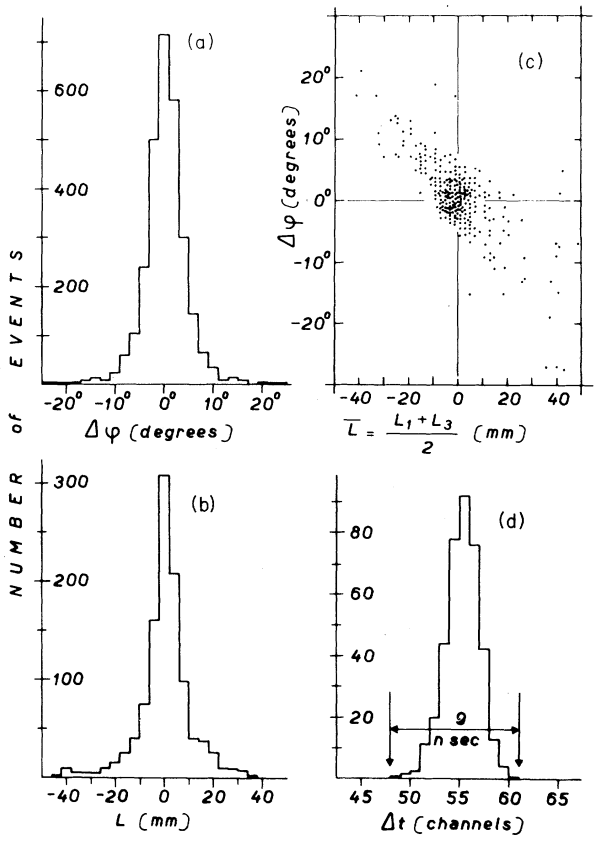

FIG. 4. Track and time analysis of a sample of $[e,e]$ events. (a) $\Delta\varphi$ distribution for in-time events; (b) L distribution for in-time events; (c) $\Delta\varphi$ vs L plot for in-time events; (d) Δt distribution for all the $[e,e]$ events coming from the source region.

mic rays, shows only the cluster corresponding to minimum ionizing particles, while the $[e,e]$ region appears practically empty [see Fig. 3(b)]. This shows that the $[e,e]$ in-time events have only a small contamination from cosmic rays.

Further, the other information we have from track reconstruction using the wire spark chambers allows us to conclude that all but a small fraction of the $[e,e]$ in-time events are e^+e^- elastic scattering events. The track analysis of in-time $[e,e]$ events is shown in Figs. 4(a)–4(c). Figure 4(a) shows the noncoplanarity angle $\Delta\varphi$ distribution, where $\Delta\varphi$ is the angle between the two planes which contain each of the two tracks and are parallel to the beam axis.[15] The $[e,e]$ events clearly appear to be coplanar (i.e., $\Delta\varphi \simeq 0$), the $\pm 3^\circ$ angular spread (HWHM) being due to spark-chamber resolution and multiple scattering in the vacuum chamber walls (1.2 g/cm^2 = 0.087X_0 of Fe) and in the telescope absorbers (12.8 g/cm^2 = 0.46X_0). In Fig. 4(b) for the particles constituting the in-time $[e,e]$ events a histogram is displayed of the distance L between their tracks and the axis of the beam. L is positive or negative according to the relative position of the particle trajectory with respect to the beam line. From this distribution (in which all four telescopes have been added) it can be seen that almost all the events appear to originate within ±5 mm (HWHM) of the beam region. Also in this case multiple scattering and spark-chamber resolution account for the observed width [the transverse dimensions of the beam are actually $\simeq(1\times1)$ mm^2]. This interpretation of the experimental widths of $\Delta\varphi$ and L distributions is confirmed in Fig. 4(c). In fact, the clear correlation observed between $\Delta\varphi$ and the average distance, $\bar{L}$, of the two tracks from the beam is what one could expect if all the events originated with $\Delta\varphi = 0$ in the (1×1) mm^2 source region, and the outcoming particles were scattered before crossing the spark chambers. Finally, from the Δt distribution of all the $[e,e]$ events, shown in Fig. 4(d), we can precisely define the interval of time in which the im-

pact of the two bunches of e^+ and e^- occurred. The peak of the distribution is as narrow as 3 nsec [full width at half maximum (FWHM)] and the fraction of events outside of the in-time interval (9 nsec wide) is absolutely negligible.

From the previous considerations we can conclude that (apart from small background subtractions discussed later; see Sec. IV B) the $[e,e]$ events are two-body events, with charged, showering particles originating in e^+e^- collisions. Thus they are e^+e^- elastic scattering events.

A reliable track analysis of the data requires that all four chambers involved in the event have correctly fired. Since the efficiency of our monogap spark chambers has been measured to be about ~0.85 (Ref. 16), there is a sizeable fraction (~50%) of $[e,e]$ events which do not have all four chambers firing. However, we have concluded from the above track analysis of the 4-chamber electron events (i.e., $[e,e]$ events in which all four chambers have fired) that practically all the $[e,e]$ in-time events that satisfy the above-mentioned pulse-height requirements are e^+e^- elastic scattering events. In particular, the presence of noncoplanar $[e,e]$ events is completely negligible. So for the evaluation of the Bhabha cross section we can use all the detected $[e,e]$ events irrespective of spark-chamber information. In this way, we have considerably higher statistics (while the background subtractions remain still quite small; see Sec. IV B below) and more importantly we avoid any problem connected with the spark-chamber inefficiencies.

During 1505 hours of running time, with an integrated luminosity $\mathcal{L} \simeq 3.5 \times 10^{35}$ cm^{-2}, we have collected a total of 5164 $[e,e]$ events in the c.m. energy range 1.4–2.4 GeV. They are listed at each c.m. energy, $E_+ + E_-$, in the third column of Table II.

B. Background Subtractions

There are two different types of background subtractions:

(1) the cosmic-ray background which can be easily experimentally determined from the number of out-of-time $[e,e]$ events (appropriately normalized according to the ratio of the widths of the out-of-time and in-time intervals) [this subtraction is of the order of ~2% (see the fourth column of Table II)];

(2) a contamination due to interactions of either beam with the residual gas in the storage ring. For the purpose of evaluating this contamination we have performed background runs with only a single beam or with two separated beams stored in the ring. In these background runs during ~600 hours we have collected a total of 64 $[e,e]$ events occurring in the in-time interval. In order to correctly subtract the contamination from electron-gas interactions from our data we must deduce the appropriate normalization factor to be applied to these background events. The value of this normalization factor was obtained by monitoring the rate of each single telescope T_i during both the background and the colliding-beam runs. The single telescope rates $\dot{T}_i$, after correction for cosmic rays, are proportional to the product of the beam currents and the residual gas density in the machine. This fact has been checked by simultaneous measurements of the single telescope rates and the single beam-gas bremsstrahlung rate $\dot{B}$. The ratio $\dot{T}_i/\dot{B}$ was found to be constant to within ~1% as a function of the beam intensity and gas pressure over the working range of this experiment. The normalization factor (which is the same regardless of which telescope T_i is used as a basis for the normalization) varies, of course, for each experimental run depending on the relative running times and the c.m. energies. The beam-gas contamination is near zero at low energy, but rises to ~8% at 2.4 GeV total c.m. energy. The average contamination for the full sample of $[e,e]$ events is ~2% (see the fifth column of Table II).

After background subtractions are performed, we are left with a total of 4939 $[e,e]$ elastic scattering events.

C. Corrections to the Data

Several small corrections must be applied to the background subtracted $[e,e]$ events:

a. Shower correction. Since the probability that an electron produces a detectable shower in the sandwich counter $(C_i + D_i)$ is not 100%, we expect that a small fraction of events $e^+e^- \to e^+e^-$ do not appear in the $[e,e]$ region of Fig. 3. To evaluate the size of this shower correction we have analyzed the events which fall in the $[\mu,e]$ regions of Fig. 3 (i.e., the events in which only one particle gives rise to a shower with a pulse height larger than $H_{i,\max}$). We find that their L and $\Delta\varphi$ distributions [see Figs. 5(a) and 5(b)] are the same as for the $[e,e]$ events, as we expect if these in-time $[\mu,e]$ events are true e^+e^- scattering events. The only difference is the presence in the $\Delta\varphi$ distribution of a long tail toward the large $\Delta\varphi$ values [see Fig. 5(c)] due to the occurrence of hadronic noncoplanar events which will be discussed in more detail in Sec. V B. After appropriate background subtractions are performed, from the number of $[\mu,e]$ events we are able to determine the probability, ϵ_μ, for an electron to have a pulse height less than $H_{i,\max}$, since the probability for an event to appear

TABLE II. Wide-angle e^+e^- elastic scattering results. The rows marked with an asterisk refer to runs in which the counters CR_3, CR_4 were set in anticoincidence with the trigger (second set of measurements, see Sec. II). Quoted errors are only statistical.

c.m. energy $E_+ + E_-$ (GeV)	Integrated luminosity (cm^{-2})	Collected $[e,e]$ events	Normalized cosmic-ray background	Normalized beam-gas background	Corrected e^+e^- Bhabha events	m small-angle monitor events	$R_{exp} = \frac{\sigma(e^+e^- \to e^+e^-)}{\sigma_{theory}}$	$\langle q^2 \rangle$ $[(GeV/c)^2]$
1.4	68×10^{32}	212	3.9 ± 1.2	0.2 ± 0.7	803 ± 47	198.4×10^3	0.967 ± 0.056	0.87
1.4*	113×10^{32}	306	5.3 ± 1.2	-0.6 ± 0.9				
1.5	52×10^{32}	141	3.6 ± 1.1	0.2 ± 0.8	1158 ± 47	308.9×10^3	1.011 ± 0.043	0.95
1.5*	280×10^{32}	738	13.6 ± 1.9	-1.6 ± 2.4				
1.6	77×10^{32}	176	4.5 ± 1.2	1.1 ± 1.2	234 ± 22	64.6×10^3	1.055 ± 0.098	1.08
1.65	114×10^{32}	187	3.8 ± 1.1	2.1 ± 1.8	242 ± 21	87.6×10^3	0.829 ± 0.073	1.14
1.7	126×10^{32}	259	3.8 ± 1.1	3.2 ± 2.2	350 ± 26	89.8×10^3	1.197 ± 0.091	1.21
1.75	135×10^{32}	192	4.2 ± 1.2	3.7 ± 2.3	251 ± 23	88.3×10^3	0.894 ± 0.083	1.29
1.8	135×10^{32}	226	3.1 ± 1.0	4.8 ± 2.6	299 ± 25	81.3×10^3	1.164 ± 0.097	1.36
1.85	260×10^{32}	417	7.7 ± 1.6	2.6 ± 2.3	1551 ± 59	377.4×10^3	1.312 ± 0.048	1.44
1.85*	420×10^{32}	825	7.2 ± 1.5	5.6 ± 10.0				
1.9	134×10^{32}	186	4.2 ± 1.2	8.6 ± 3.2	231 ± 21	68.3×10^3	1.126 ± 0.105	1.52
2.0	290×10^{32}	328	7.6 ± 1.6	30.2 ± 6.0	389 ± 31	128.2×10^3	1.025 ± 0.082	1.68
2.4	148×10^{32}	102	3.6 ± 1.1	4.0 ± 2.7	1102 ± 55	302.2×10^3	1.228 ± 0.060	2.42
2.4*	1147×10^{32}	869	15.1 ± 2.1	69.5 ± 17.9				
Totals	3499×10^{32}	5164	91.2 ± 5.3	133.6 ± 22.5	6610 ± 123	1795.9×10^3		

in a $[\mu,e]$ region is $2\epsilon_\mu(1-\epsilon_\mu)$. This has been done at each c.m. energy, since the value of ϵ_μ clearly depends on the energy of the electron: We found experimentally that it ranges from 4.6% at $E_\pm = 1.2$ GeV up to 12.6% at $E_\pm = 0.7$ GeV. The experimental values of ϵ_μ and the corresponding correction factors $F_S = (1-\epsilon_\mu)^{-2}$ to be applied for this effect to the $[e,e]$ events are listed in the second and third columns of Table III at each primary electron energy $E_\pm$.

b. Cosmic-ray veto correction. In the first set of measurements (see Sec. II, and Tables I and II) an e^+e^- event is lost if one of the electrons passes through the 22 cm of Fe absorber and produces an anticoincidence pulse in counter CR_1 or CR_2. In the second set of measurements with a second roof of absorber and two additional counters CR_3 and CR_4 placed on the top of the apparatus, as de-

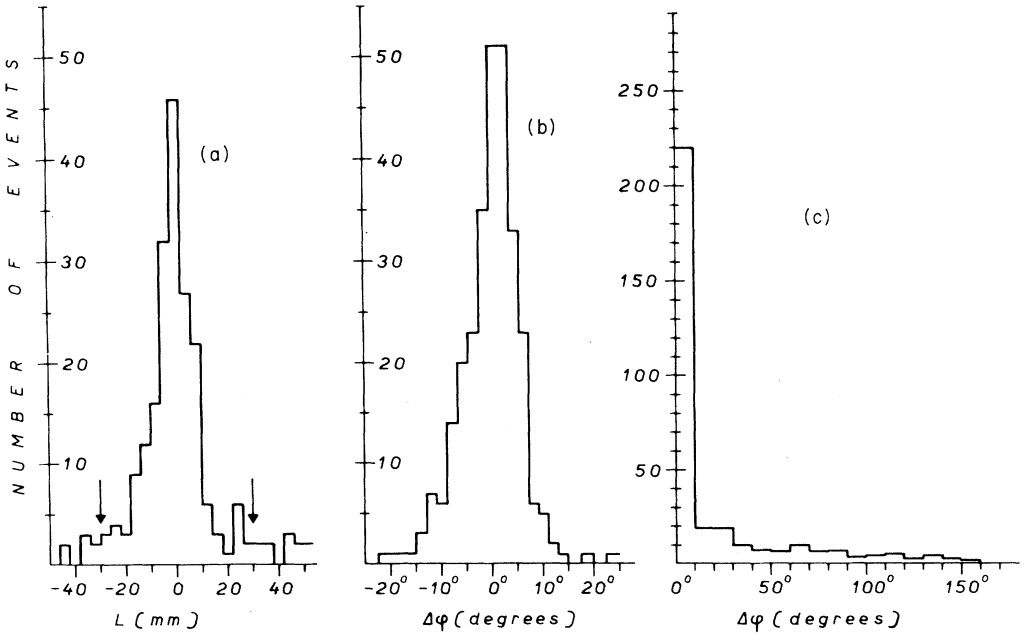

FIG. 5. Track analysis of a sample of in-time $[\mu,e]$ events. (a) L distribution; (b) $\Delta\varphi$ distribution in the region around 0°; (c) total $|\Delta\varphi|$ distribution.

TABLE III. Shower corrections and anticoincidence corrections. First column: single beam energy, $E_\pm$; second column: measured shower inefficiency, ϵ_μ; third column: shower correction factor, F_S; fourth column: measured fraction of marked events, f; fifth column: anticoincidence correction factor, F_{AC}.

	Shower correction		Anticoincidence correction	
$E_\pm$ (GeV)	ϵ_μ (%)	F_S	f (%)	F_{AC}
0.7	12.61±0.34	1.31±0.07		1.039±0.017
0.725			4.2±0.7	1.044±0.018
0.75	7.94±0.20	1.18±0.06		1.049±0.018
0.8	9.83±0.24	1.23±0.06		1.060±0.015
0.825	8.33±0.17	1.19±0.05		1.066±0.016
0.85	9.83±0.20	1.23±0.05		1.072±0.017
0.875	8.71±0.22	1.20±0.06		1.078±0.017
0.9	8.71±0.18	1.20±0.05		1.082±0.020
0.925	6.34±0.22	1.14±0.08	8.2±1.7	1.089±0.020
0.95	7.15±0.15	1.16±0.05		1.094±0.022
1.0	6.74±0.15	1.15±0.05		1.105±0.024
1.20	4.65±0.17	1.10±0.08	13.3±2.6	1.153±0.035

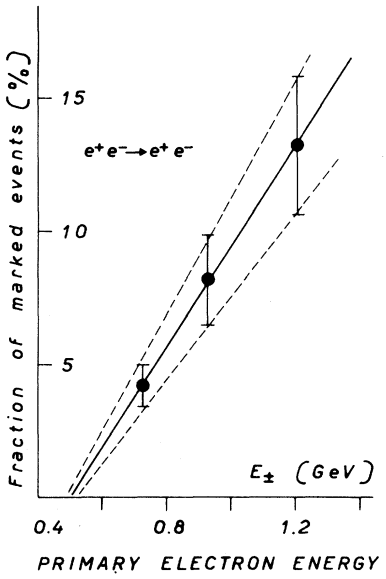

FIG. 6. The fraction of marked $[e, e]$ events as a function of the primary electron energy $E_\pm$.

scribed in Sec. II (see also Fig. 1), we have directly evaluated the fraction of e^+e^- events that were lost due to anticoincidence in CR_1 or CR_2. This was done by measuring the fraction, f, of marked e^+e^- events (i.e., not vetoed by CR_3 or CR_4, but in which CR_1 or CR_2 were triggered). Since the number of e^+e^- events vetoed by CR_3 or CR_4 was determined to be negligible, f represents directly the fraction of events lost in the first set of measurements, and was found to vary linearly from 4.2% at $E_\pm = 0.725$ GeV to 13.3% at $E_\pm = 1.2$ GeV (see Fig. 6). For the energies covered in the first set of measurements but not in the second, a linear interpolation of f was used. The values of f and the correction factors $F_{AC} = (1-f)^{-1}$ we have used are listed in the fourth and fifth columns of Table III.

c. Multiple-scattering correction. The geometrical acceptance is reduced by a small factor due to multiple scattering near the boundary of the telescopes. We have calculated the correction for these losses to be approximately energy-independent and equal to (+2.5±2)%.

d. Geometrical misalignment correction. Due to possible misalignments of the apparatus with respect to the source position, an uncertainty has to be assigned to the geometrical acceptance. The corresponding correction to be applied to measured events is (+3±3)%.

e. Radiative corrections. Calculated radiative corrections turn out to be, in our case, negligible (<2%).

We summarize the situation on the corrections as follows:

(a) Shower corrections: ranging from +31% at 1.4 GeV $E_+ + E_-$ c.m. energy to +10% at 2.4 GeV (experimentally measured);

(b) Cosmic-ray veto corrections: ranging from +3.9% at 1.4 GeV to +15.3% at 2.4 GeV (experimentally measured);

(c) Multiple-scattering correction: (+2.5±2)% (calculated value);

(d) Geometrical misalignment correction: (+3±3)% (calculated value);

(e) Radiative corrections: negligible (<2%, calculated value).

All the above corrections have been applied to the number of collected events, after background subtractions have been performed. The corrected numbers of e^+e^- Bhabha-scattering events are listed in the sixth column of Table II. However, those systematic uncertainties which do not depend on the energy (associated with multiple-scattering and geometrical misalignments corrections) are not included in the quoted errors. They will be taken into account in the over-all normalization uncertainty shown in Fig. 8.

D. Comparison with Theory

According to QED, the elastic electron-positron scattering is described at the lowest order by the diagrams shown in Fig. 7.

The four-momentum squared of the virtual photon is spacelike in the scattering diagram and timelike in the annihilation diagram. In the c.m.

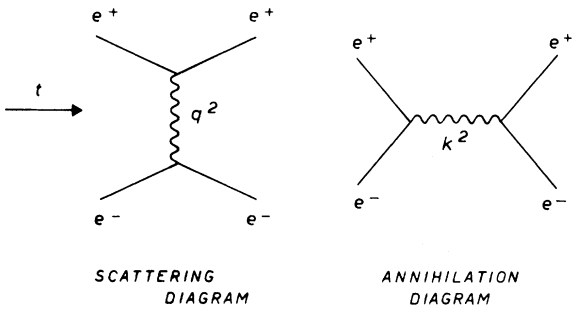

FIG. 7. Feynman diagrams for e^+e^- elastic scattering at lowest order.

system they are respectively given by

$$q^2 = +4E_\pm^{\,2}\sin^2(\tfrac{1}{2}\theta) \quad \text{and} \quad k^2 = -4E_\pm^{\,2},$$

where $E_\pm$ is the energy of either the electron or the positron and θ is the scattering angle.

The resulting cross section (Bhabha cross section) can be written as

$$\left(\frac{d\sigma}{d\Omega}\right)_{\text{Bhabha}} = \frac{r_0^{\,2}}{8}\left(\frac{m_e}{E_\pm}\right)^2 [S(q^2,k^2)+I(q^2,k^2)+A(q^2,k^2)], \tag{4.1}$$

where m_e and r_0 are the mass and the classical radius of the electron,

$$S(q^2,k^2) = \frac{k^4+(q^2+k^2)^2}{q^4}$$

is the contribution of the scattering diagram,

$$A(q^2,k^2) = \frac{q^4+(q^2+k^2)^2}{k^4}$$

is the contribution of the annihilation diagram, and

$$I(q^2,k^2) = 2\frac{(q^2+k^2)^2}{k^2q^2}$$

is the interference term between the two diagrams. Of course, the Bhabha formula is only a first-order description of the electron-positron scattering process and we must consider terms from higher-order diagrams, that is,

$$\left(\frac{d\sigma}{d\Omega}\right)_{\text{QED}} = \left(\frac{d\sigma}{d\Omega}\right)_{\text{Bhabha}} + \text{radiative corrections}. \tag{4.2}$$

These radiative corrections can be separated into virtual (internal) and real (external) photon contributions whose divergent parts cancel to order α^3.[17] These contributions have been calculated for wide-angle electron-positron scattering,[18] and for our apparatus result in a small correction ($<2\%$) due to the compensation of internal and external contributions, each of which can be as large as 10%.

Experimentally we wish to verify whether or not the e^+e^- elastic scattering is actually described by the pointlike elastic scattering cross section $(d\sigma/d\Omega)_{\text{QED}}$. We have therefore considered the ratio (R_{exp}) of the experimentally measured cross section to the pointlike cross section integrated over our angular acceptance $\Delta\Omega$:

$$R_{\text{exp}} = \frac{\int_{\Delta\Omega}(d\sigma/d\Omega)_{\text{exp}}\,d\Omega}{\int_{\Delta\Omega}(d\sigma/d\Omega)_{\text{QED}}\,d\Omega}. \tag{4.3}$$

Of course, if the scattering process is actually described by the pointlike cross section, this ratio will be unity.

In order to be able to interpret any deviations of R_{exp} from unity we will consider the most general form (at first order) that can be assumed for a non-pointlike elastic scattering cross section consistent with Lorentz and gauge invariance. Since the electron anomalous magnetic moment μ_a is small ($\mu_a/m_e \ll e$) (Ref. 19), we can write

$$\left(\frac{d\sigma}{d\Omega}\right)_{\text{modified}} = \frac{r_0^{\,2}}{8}\left(\frac{m_e}{E_\pm}\right)^2 \{|G(q^2)|^2 S(q^2,k^2) + \text{Re}[G(q^2)G(k^2)]I(q^2,k^2) + |G(k^2)|^2 A(q^2,k^2)\}, \tag{4.4}$$

where $G(q^2) = F^2(q^2)M(q^2)$ is the product of a possible electron form factor squared, $F^2(q^2)$, and a possible modification factor, $M(q^2)$, to the photon propagator. For our apparatus centered around $\theta = 90^\circ$ the contribution from the scattering term dominates that of the interference and annihilation terms. In this case, if we also neglect the radiative correction contribution which has been shown to be small in the pointlike case, we find $R_{\text{exp}} \simeq \langle|G|^2\rangle$. $\langle|G|^2\rangle$ is the weighted average of $|G|^2$ over the experimental apparatus. Clearly a test of the validity of QED (i.e., $|G|^2 = 1$) is therefore equivalent to verifying that $R_{\text{exp}} \equiv 1$, while a measurement of this ratio different from unity can directly be associated with the average value of the form factor $\langle|G|^2\rangle$.

We can now rewrite the equation (4.3) in terms of the detected wide-angle scattering events, $n_{e^+e^-}$, and the monitor events, m (see Sec. III), as follows:

$$R_{\exp}=\frac{n_{e^+e^-}/\mathcal{L}}{\int_{\Delta\Omega}(d\sigma/d\Omega)_{\mathrm{QED}}\,d\Omega}$$

$$=\frac{n_{e^+e^-}}{m}\,\frac{\int_M(d\sigma/d\Omega)_{\mathrm{QED}}\,d\Omega}{\int_{\Delta\Omega}(d\sigma/d\Omega)_{\mathrm{QED}}\,d\Omega}\,. \tag{4.5}$$

The last step makes use of the determination of the integrated luminosity, $\mathcal{L}$, through the measurement of the yield m in the monitor apparatus, M (Ref. 20), i.e.,

$$m=\mathcal{L}\int_M\left(\frac{d\sigma}{d\Omega}\right)_{\mathrm{QED}}d\Omega\,, \tag{4.6}$$

where we have made the hypothesis that e^+e^- scattering is well described by QED (pointlike) at the small momentum transfers (<100 MeV/c) involved in the monitor apparatus. Again, in the case of the monitor, radiative corrections to the Bhabha cross section have been calculated[21] and are found to be small ($<2\%$).

Expressing $R_{\exp}$ as a ratio of wide-angle events to monitor events minimizes the sensitivity of our results to the actual value of the finite, energy-dependent, source length[9] $\bar{l}_z$, since the efficiencies of both the monitor and our experimental apparatus have approximately the same dependence on $\bar{l}_z$. Additional care must be taken in the evaluation of (4.5) to symmetrize the QED cross section in θ and $\pi-\theta$ since our apparatus does not permit charge recognition.

The results of the evaluation of $R_{\exp}$ for each measured c.m. energy are shown in Fig. 8. The statistical errors for each point are shown as bars, while the systematic, energy-dependent uncertainties due to erratic fluctuations in the monitor (±7%) are indicated as small rectangles. The systematic uncertainties due to multiple-scattering corrections (±2%), geometrical misalignment (±3%), and an over-all monitor normalization (±5%) have

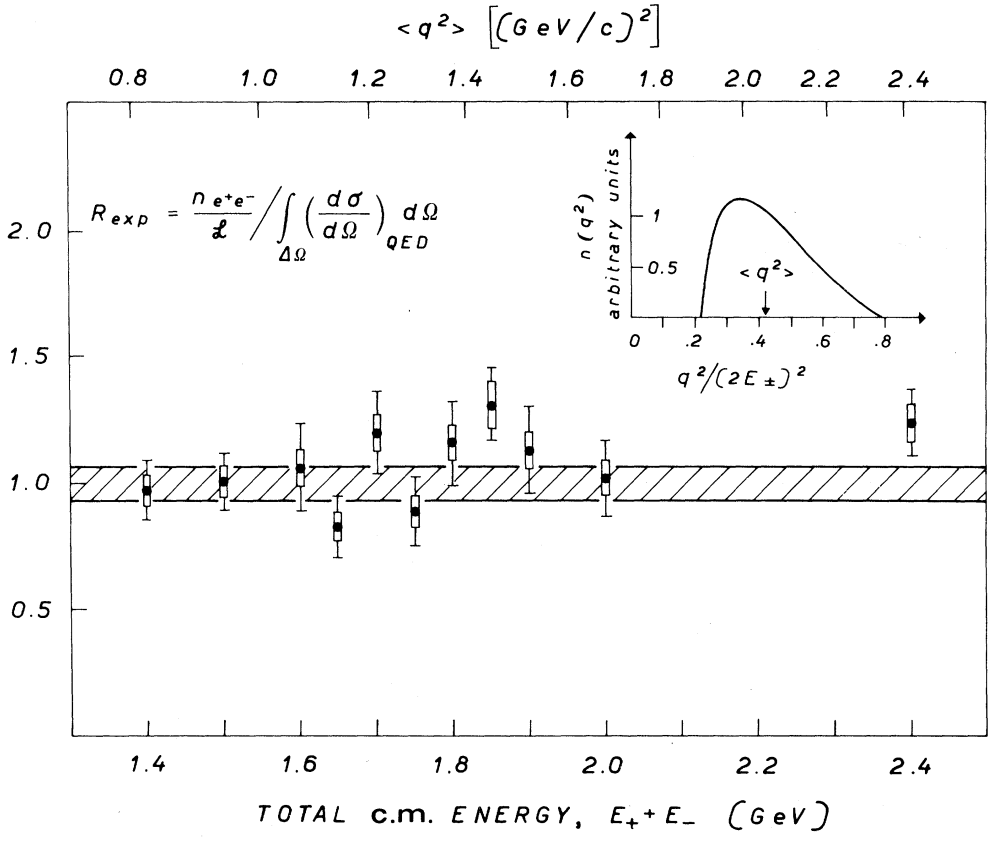

FIG. 8. Wide-angle e^+e^- elastic scattering data compared as a function of the total c.m. energy with QED theory. For each experimental point statistical errors are shown as bars, while systematic uncertainties are indicated as small rectangles. The dashed band (±6.5%) about $R_{\exp}=1.0$ indicates those systematic uncertainties which are the same at all the energies. The q^2 acceptance of the apparatus weighted on the Bhabha cross section is shown in the upper right-hand corner.

been indicated by a dashed band (±6.5%) centered about $R_{exp}=1$. Shown in the same figure is the q^2 acceptance $n(q^2)$ of the apparatus, weighted by the Bhabha cross section.

Our data do not indicate any deviation from $\langle|G(q^2)|^2\rangle=1$ over the range of q^2 explored and they are fitted very well ($\chi^2=10.8$ for 10 degrees of freedom) by a constant value

$$\overline{R}_{exp}=1.05\pm0.04\ (\pm6.5\%\ \text{systematic})$$

which must be compared to the pointlike prediction $R=1.00$.[22]

V. REACTION $e^+e^-\to a^\pm+b^\pm+$ANYTHING

A. Selection of the Events

We will now discuss events from the reaction

$$e^+e^-\to a^\pm+b^\pm+\text{anything}, \tag{5.1}$$

where $a^\pm$ and $b^\pm$ are any charged particles. The master coincidence which triggers the apparatus requires the presence of at least two charged particles ($a^\pm$ and $b^\pm$) detected in two different telescopes.

Since reaction (5.1) is not a two-body reaction, we have restricted ourselves to the analysis of noncoplanar events, which are defined as follows:

(a) more than two charged particles detected, each entering a different telescope, and having a pulse height $H_i\geq H_{i,\min}$;

(b) only two charged particles detected with the restrictions that their pulse heights (H_i,H_j) (greater than the respective low-pulse-height cuts $H_{i,\min}$ and $H_{j,\min}$) are not in the region $[e,e]$ of the pulse-height plot (see Fig. 3 for reference); and further their noncoplanarity angle $|\Delta\varphi|$ (defined in Ref. 15, Sec. IV A) is $\geq13^\circ$;

(c) only two charged particles detected with their pulse heights in the $[e,e]$ region of the pulse-height plot, and a noncoplanarity angle $|\Delta\varphi|\geq40^\circ$.

The larger $\Delta\varphi$ cut of selection criterion (c) was chosen in order to exclude from our sample of events any contamination from the radiative reaction $e^+e^-\to e^+e^-\gamma$. However, the number of the noncoplanar events selected with criterion (c) was only a small fraction (~7%, see Sec. V B) of the observed noncoplanar events.

The evaluation of the noncoplanarity angle $\Delta\varphi$ between two particles requires information on the projected paths of the particles and therefore the positions of the sparks in both monogap magnetostrictive chambers of the two telescopes traversed by the particles. An event with this complete determination of track positions is designated hereafter as a 4-chamber event or 4-chm. Since our monogap spark chambers have an efficiency of ~85% (see Ref. 16), confining ourselves to 4-chm events rejects ~50% of all the events. We will see, however, that we can analyze those events in which the spark in one of the four chambers is missing (3-chamber events, or 3-chm) by making an appropriate hypothesis. The analysis of these 3-chm events has been performed and is presented after that of the 4-chm events.

For completeness, we recall (see Sec. II) that we have performed two different sets of measurements. During the first set, the counters CR_1, CR_2 were used as veto counters in the trigger; in the second set of measurements, counters CR_3, CR_4 were added and used as veto counters while counters CR_1, CR_2 were only recorded. In order to have a homogeneous set of data we do not include in the following analysis events in which a particle crosses the 22 cm Fe and stops in the lead absorber between CR_1, CR_2 and CR_3, CR_4 (marked events). We have used the number of detected marked events to obtain information on the penetration of the detected particles.

1. *4-chamber Events: Analysis and Background Subtractions*

4-chamber events are defined as those for which the projections of the tracks on a plane orthogonal to the beam axis of at least two charged particles are completely determined. That is, by definition, in a 4-chm event complete reconstruction is possible for at least two charged-particle trajectories (if other particles are present in other telescopes their track reconstruction may or may not be possible). For each of the reconstructed tracks the minimum distance from the beam axis, L_i, and the azimuthal angle, φ_i (see Sec. II), can be evaluated. Using these azimuthal angles we can select the noncoplanar 4-chm events.

Among these events, those from reaction (5.1) must occur in-time with the beam-beam impact. From the analysis of the Bhabha events we have already determined the in-time interval, Δt (see Fig. 4, Sec. IV A). In addition they must originate in the region of intersection of the electron-positron bunches (source region) and therefore the distribution of the distances from the beam axis of the detected particle tracks has been studied.

In Fig. 9 a two-dimensional sample plot of noncoplanar events in a plane L_i, L_j is presented. Figure 9(a) refers to in-time events, and shows a clear clustering of events about the origin (the projection of the beam axis) in addition to a cosmic-ray and machine background scattered over the entire plane. Figure 9(b) shows the same plot for a sample of out-of-time events. In this case a clustering near the origin is not present since the out-of-time events are cosmic rays. In Fig. 10(a) we

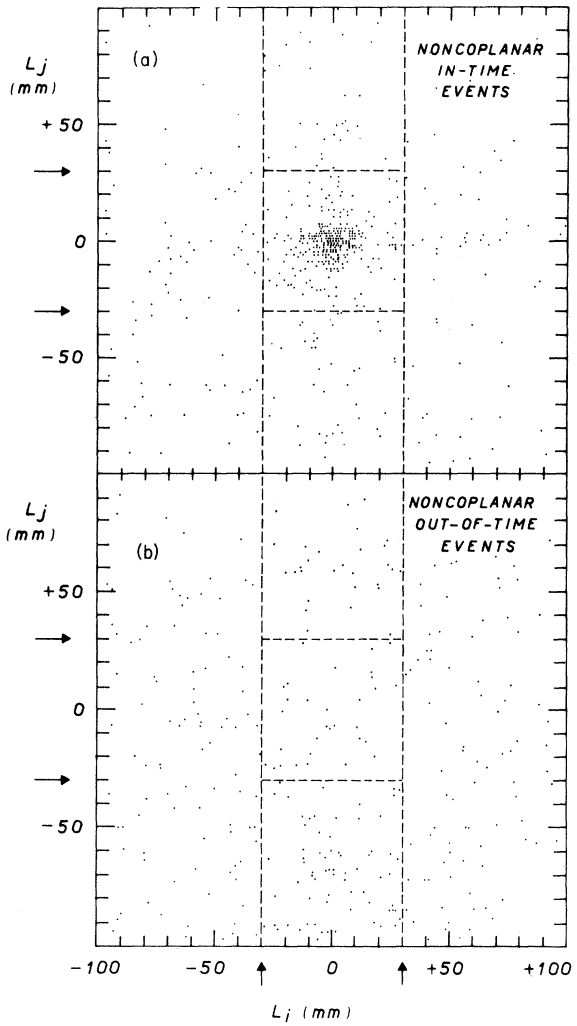

FIG. 9. Plots of L_i vs L_j for a sample of 4-chm noncoplanar events. (a) In-time events; (b) out-of-time events.

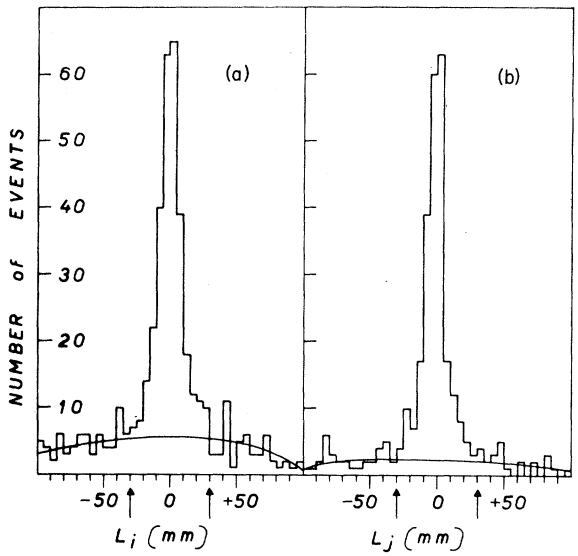

FIG. 10. Projections of the sample plot in Fig. 9(a). (a) All the events projected on the L_i axis; (b) the events for which $|L_i| \leq 30$ mm, projected on the L_j axis.

have projected the plot of Fig. 9(a) on the L_i axis. There is a clear peak of events coming from the source. A smooth interpolation under the peak of the background tails would indicate a background contamination of roughly 20% to the events coming from the source. However, if we project on the L_j axis those events for which $|L_i| \leq 30$ mm [Fig. 10(b)], the peak of the events from the source is now superimposed over a somewhat smaller background (interpolated value ~10%). As was the case for the Bhabha events, the source width (~7.5 mm) is what one would expect from spark-chamber resolution and multiple scattering in the vacuum-chamber walls and in the telescope absorbers. From the analysis of these types of distributions, we have defined as in-source events those for which $|L_i|$ and $|L_j|$ are both $\leq$30 mm. Figure 11(a) shows the L_j distribution [equivalent to the distribution of Fig. 10(b)] for all our 4-chm, noncoplanar, in-time events. The Δt distribution in Fig. 11(b) for the 4-chm, noncoplanar, in-source events clearly demonstrates that practically all the events are in-time with the beam impact.

We have collected in the energy range $E_+ + E_- = 1.4$–2.4 GeV a total of 428 4-chm noncoplanar events which are in-time with the beam-beam impact and come from the source region. These events are listed in the second column of Table IV and are divided according to their detected configuration: i.e., two charged tracks detected ($2\mathcal{T}$, following the notations of Sec. II); two charged plus one neutral ($2\mathcal{T}+\mathcal{N}$); etc. From these events we must subtract cosmic-ray and machine associated background. The cosmic-ray contribution to the in-time, in-source, noncoplanar events can be calculated at each energy by appropriately normalizing the corresponding out-of-time events. The normalization factor was determined from the ratio of in-time to out-of-time events during machine-off background runs. The cosmic-ray contamination for these 4-chm events was quite small at all energies, the average being ~2.5%. The cosmic-ray subtraction for each configuration is listed in the third column of Table IV.

Since the machine background is peaked in the source region due to beam-gas interactions, a smooth interpolation of the background tails of the L distribution is not a correct procedure to determine the total background contamination of the in-source events. The amount of machine associated background was determined by background runs

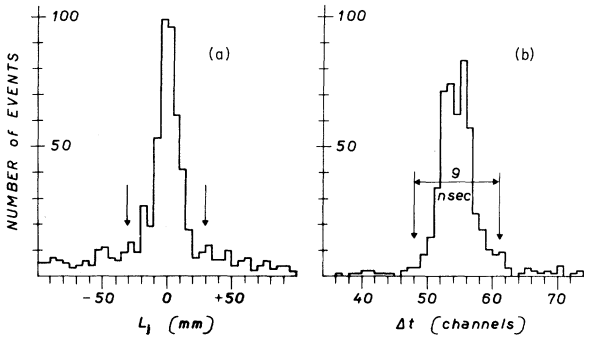

FIG. 11. L_j and Δt distributions for all the 4-chm noncoplanar events. (a) L_j distribution for the in-time events for which $|L_i| \leq 30$ mm; (b) Δt distribution for in source ($|L_i|, |L_j| \leq 30$ mm) events.

with one beam or two separated beams in the storage ring (see Sec. IV B 2). During 600 hours of these runs we collected 43 events which satisfied the selection criteria for noncoplanar events. After cosmic-ray subtraction, we normalized these events for each energy to our measurement runs, as was discussed in the case of wide-angle e^+e^- measurements. The average contamination of the in-source, in-time events due to these machine associated events was $(23 \pm 4)\%$. Practically all of this background was in the 2τ event configuration (see the fourth column, Table IV). As a function of c.m. energy this contamination was approximately constant and $\leq 5\%$ in the energy range 1.4–1.9 GeV, but increased sharply to a maximum of ~75% at 2.4 GeV. We note that with the normalization procedures used for the background subtractions (within the statistical errors) we can account for all of the out-of-source events in the tails of the L distribution [see Fig. 11(a)].

After cosmic-ray and machine background subtractions, the total number of noncoplanar 4-chm events is 317. They are listed by configuration in the fifth column, Table IV.

2. *3-chamber Events: Analysis and Background Subtractions*

For these events only one charged-particle trajectory is completely defined by a spark in both chambers of the triggered telescope T_i. The second (and possibly the third) particle trajectory is not completely determined, since a spark is missing in one chamber of its telescope T_j. In order to determine the trajectory of this second (third) particle we make the hypothesis that the event originates at that point of the trajectory, measured in telescope T_i, which is closest to the beam axis. In this way we can determine the azimuthal angle, φ_j, for the particle trajectories with only one spark. The resulting uncertainty in the determination of φ_j is quite small ($\delta\varphi_j < 2^\circ$) for those events physically originating in the source region. On the other hand some events physically originating outside the source region, which are due to cosmic-ray and machine background, by this procedure can be added to our sample of in-source events. In fact the reconstructed origins of the 3-chm events are closer to the beam axis than the true origins. Therefore the only result of this procedure is a larger background contamination to be subtracted from our 3-chm events.

The analysis of the 3-chm events can then proceed as for 4-chm events. The only difference is that L_i vs L_j two-dimensional plots cannot be compiled. However, it is possible to construct the one-dimensional distribution of events as a function of L_i without any condition on L_j (which is not measured). This distribution, which is the equivalent of the one shown in Fig. 10(a) for 4-chm events, is given in Fig. 12(a). The in-source 3-chm events are now defined as those for which $|L_i| \leq 30$ mm. By comparing the L distribution of Fig. 11(a) (4-chm events) with Fig. 12(a), we confirm that this analysis of the 3-chm events simply results in a somewhat higher background contamination. Figure 12(b), which shows the Δt distribution for the 3-chm noncoplanar events coming from the source, allows us to conclude that most of the additional background is due to cosmic rays.

We have collected a total of 609 3-chm events which are noncoplanar, in-time with the beam-beam impact, and come from the source. They refer to several c.m. energies between 1.4 and 2.4 GeV and are listed in the sixth column of Table IV according to their detected configurations.

Background subtractions from the 3-chm events have been performed in the same way as for the 4-chm events. Cosmic-ray contamination has been evaluated by selecting and appropriately normalizing the 3-chm out-of-time events. This cosmic-ray contamination ranges from 17% at 2.4 GeV to 40% at 1.4 GeV, the average contamination being ~25%. The machine background to be subtracted from the 3-chm, in-time, in-source, noncoplanar events has been measured to have the same value within the errors, energy by energy, as for the 4-chm events [average value $(28 \pm 4)\%$]. Cosmic-ray and machine background subtractions for the 3-chm events are listed in the seventh and eighth columns of Table IV.

The 288 noncoplanar 3-chm events remaining after background subtractions are listed in the ninth column of Table IV according to their different detected configurations.

B. Nature of the Observed Particles

From the analysis we have discussed in the previous sections a total of 605 (3-chm+4-chm) events remain after subtracting cosmic-ray and machine background (see the tenth column of Table IV). These noncoplanar events originate in the source region and are in-time with the beam-beam impact, i.e., they come from the reaction

$$e^+e^- \rightarrow a^\pm + b^\pm + \text{anything}.$$

In this section we will discuss the nature of these produced particles. The information made available by our apparatus is not sufficient to determine the nature of each individual detected particle; however, some statistical information can be extracted from the experimental distributions.

First, let us consider the pulse-height information from the sandwich counters $(C_i + D_i)$. In Figs. 13(a) and 13(b) pulse-height spectra of the charged particles $\mathcal{T}_1$ detected in telescope T_1 are shown (the distributions in the other telescopes are the same within the errors). The pulse-height spectrum of particles associated with the detected noncoplanar events [Fig. 13(b)] is compared with the spectrum of minimum-ionizing particles (cosmic-ray) and high-energy electrons from Bhabha scattering [Fig. 13(a)]. The distribution of the noncoplanar events is quite similar to the cosmic-ray spectrum although it shows a nonnegligible tail towards the larger pulse heights. However, by compiling the two-dimensional plot H_j vs H_i for the in-time, noncoplanar events coming from the source, we have checked that the great majority of the events (~93%) do not show any correlation between large pulse heights in the different telescopes. In fact (using the definitions of Sec. IV A, see Fig. 3 for references) 61% of the events have their pulse heights (H_i, H_j) in the $[\mu, \mu]$ region of the pulse-height plot, 32% in the $[\mu, e]$ region, and only ~7% in the $[e, e]$ region. These percentages correspond to the ~19% large pulse-height tail in the noncoplanar events distribution of Fig. 13(b). A large fraction of this tail is due to the presence of more than one particle in the same telescope. Actually, from the experimental numbers of events with more than two detected particles (see Table IV), we estimate that ~14% of our events have two particles in the same telescope. Moreover, if the detected particles were pions, the remaining 5% of events in the tail could be easily accounted for due to the following effects: nuclear interactions in the sandwich counters and greater ionization by low-energy pions. We conclude that the bulk (>95%) of the detected particles are not high-energy electrons, and that the pulse-height spectrum is compatible with all of them being pions.

TABLE IV. List of 4-chm and 3-chm noncoplanar events and background subtractions for the detected configurations.

Detected configuration	Collected events	4-chm noncoplanar events			3-chm noncoplanar events			4-chm+3-chm noncoplanar events after background subtractions
		Normalized cosmic-ray background	Normalized beam-gas background	Noncoplanar events after background subtractions	Collected events	Normalized cosmic-ray background	Normalized beam-gas background	Noncoplanar events after background subtractions
$2\mathcal{T}$	333	8.4 ±1.6	95.6±15.0	229.0±24.0	513	133.8±6.7	157.2±21.7	222.0±32.0	451.0±40.0
$2\mathcal{T}+1\gamma$	49	0.6 ±0.4	4.8±3.3	43.6±7.8	59	11.1±1.9	11.9±5.9	36.0±9.9	79.6±12.6
$2\mathcal{T}+2\gamma$	3	0.0 ±0.35	0.0±2.0	3.0±2.7	8	0.8±0.7	3.3±2.0	3.9±3.5	6.9±4.4
$3\mathcal{T}$	39	1.1 ±0.6	0.0±2.0	37.9±6.6	25	5.4±1.2	−3.8±2.4	23.4±5.7	61.3±8.7
$3\mathcal{T}+1\gamma$	4	0.0 ±0.35	0.0±2.0	4.0±2.9	4	0.6±0.5	0.8±2.0	2.6±2.9	6.6±4.1
Totals	428	10.15±1.9	100.4±16.0	317.5±26.0	609	151.7±7.2	169.4±23.0	287.9±34.3	605.4±43.1

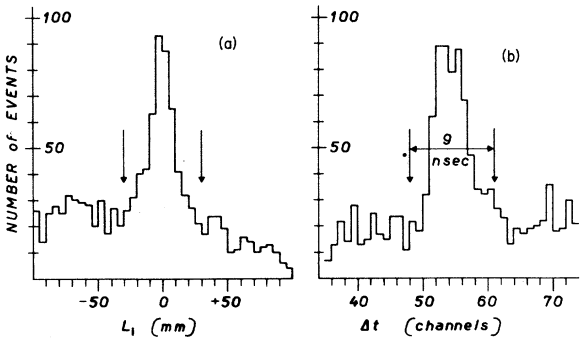

FIG. 12. L_i and Δt distributions for all the 3-chm noncoplanar events. (a) L_i distribution of the measurable track for in-time events; (b) Δt distribution for in-source events.

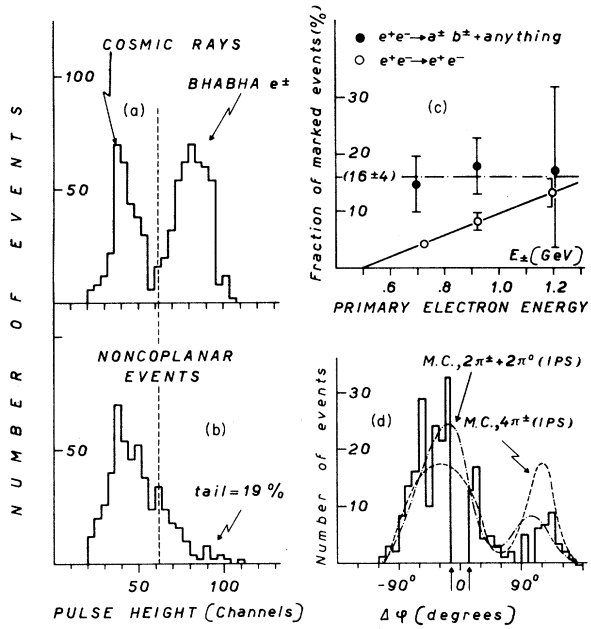

FIG. 13. (a) Cosmic-ray and Bhabha electrons pulse-height spectra in telescope T_1; (b) pulse-height distribution of in-time, in-source, noncoplanar events in telescope T_1; (c) fraction, f_M, of marked noncoplanar and Bhabha events; (d) $\Delta\varphi$ distribution of the two charged track, $2\mathcal{T}$, background-subtracted, 4-chm noncoplanar events compared with an IPS Monte Carlo calculation for two possible pion final states.

Independent experimental information on the nature of the detected particles is obtained by measuring their penetration through the 22-cm Fe absorber on top of the apparatus. In Fig. 13(c) we have plotted, as a function of the primary electron energy $E_\pm$, the fraction f_M of the background subtracted noncoplanar events in which a particle crosses the 22-cm Fe and stops between CR_1, CR_2 and CR_3, CR_4 (marked events). In the same figure the fraction of marked Bhabha electrons (see Sec. IV C) is also plotted. The number of marked Bhabha events decreases to zero at low energy and we can thus conclude that electrons with energy smaller than 500 MeV have a negligible probability (<1%) to cross the Fe absorber and to give a mark. On the other hand, the fraction f_M of marked noncoplanar events does not appear, within the large errors, to have a strong energy dependence, its average value being $(16 \pm 4)\%$. To give a feeling for such a figure, we have calculated as 16% the probability of a ~400 MeV pion entering one of the top telescopes to be marked. Furthermore, we have performed a Monte Carlo calculation (see Appendix A) which shows that, at $E_\pm = 0.7$ GeV, no reasonable pion final state would result in a value of f_M greater than 16%. This indicates that at 1.4 GeV c.m. energy the possible contamination of low-energy (<500 MeV) electrons must be very low. Also at the higher energies the measured values of f_M are consistent with a major part of the detected particles being pions. As will be discussed in Sec. V D, the experimental values of f_M will be used as one of the parameters of our best-fit procedure in order to extract information on the relative contribution from the possible different production channels.

Additional information on the nature of the particles associated with the detected noncoplanar events can be obtained from the distribution of the $\Delta\varphi$ (noncoplanarity) angle. In Fig. 13(d) the $\Delta\varphi$ distribution of the 4-chm noncoplanar events in the $2\mathcal{T}$ configuration (the statistically most significant) is shown. The 3-chm noncoplanar events have a similar $\Delta\varphi$ distribution. It is worthwhile to note that this distribution is not symmetric with respect to $\Delta\varphi = 0$. This is only due to our definition of the $\Delta\varphi$ sign, which was chosen (see Ref. 15) in order to be directly related to the actual geometrical configuration of the event.[23] For reference we have also plotted in Fig. 13(d) the statistical $\Delta\varphi$ distribution expected for the reaction $e^+e^- \to \pi^+\pi^-\pi^0\pi^0$ and $e^+e^- \to \pi^+\pi^-\pi^+\pi^-$ (phase-space Monte Carlo calculation, see Appendix A). The general features of the experimental $\Delta\varphi$ distribution are quite similar to the statistical ones, especially around $\Delta\varphi = 0$. That is, the $\Delta\varphi$ distribution of noncoplanar events is compatible with some admixture of final states produced with a statistical angular distribution. In Sec. V D we will discuss this point in a more quantitative way.

We now will use the $\Delta\varphi$ distribution in order to conclude that our sample of noncoplanar events does not contain a significant contribution from a particular nonhadronic process, namely,

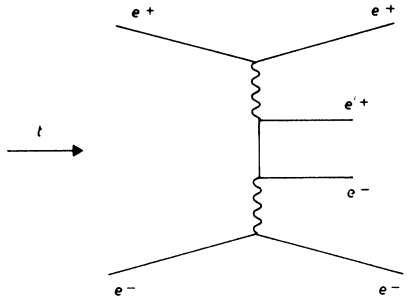

FIG. 14. Two-photon interaction diagram for the reaction $e^+e^- \to e^+e^-e^{+\prime}e^{-\prime}$.

$$e^+e^- \to e^+e^-e^+e^- . \tag{5.2}$$

Actually this is the only plausible process which could produce low-energy noncoplanar electrons, and it is foreseen to occur, at a relatively high rate, through the diagram shown in Fig. 14. According to this diagram, the e^+ and e^- in the final state are scattered in a small cone around the beam direction, while the produced e'^- and e'^+ have a peculiar $\Delta\varphi$ distribution, since the cross section $d\sigma/d(\Delta\varphi)$ for this reaction is strongly peaked around $\Delta\varphi = 0$ ($\Delta\varphi$ being the noncoplanarity angle between e'^- and e'^+). In Fig. 15(b) we have plotted the cross section $d\sigma/d(\Delta\varphi)$ of our noncoplanar events ($|\Delta\varphi| \geq 13°$). This was obtained as a ratio between the experimental distribution of Fig. 13(d) and the geometrical detection efficiency of our apparatus, $\epsilon_g(\Delta\varphi)$, to detect a two-track configuration with relative noncoplanarity angle $\Delta\varphi$. The experimental values of $d\sigma/d(\Delta\varphi)$ appear to be quite constant, within the errors, proving that the contribution from the reaction $e^+e^- \to e^+e^-e^+e^-$ does not extend, with appreciable tails, outside the region $|\Delta\varphi| < 13°$. In Fig. 15(a) we have drawn the theoretical cross-section shape for the reaction (5.2) calculated according to Baier and Fadin.[24] When normalized to give the maximum 13° peaking possible within our indicated errors, this curve allows at most a 10% contamination to our sample of noncoplanar events.

We cannot only exclude a large contamination (for $|\Delta\varphi| \geq 13°$) from the reaction $e^+e^- \to e^+e^-e^+e^-$, but from similar considerations, we can set an upper limit of ~10% for the total possible contamination from processes with a $\Delta\varphi$ distribution strongly peaked around $\Delta\varphi = 0$; i.e., $e^+e^- \to e^+e^-e^+e^-$, $e^+e^- \to e^+e^-\pi^+\pi^-$ (Ref. 25), $e^+e^- \to e^+e^-\mu^+\mu^-$, etc.

We summarize the conclusions of this section as follows. The detected particles associated with our noncoplanar events originating from the reaction $e^+e^- \to a^\pm + b^\pm$ + anything are of hadronic nature, ~10% being an upper limit for a possible contamination of electrons. In particular the contribution from the reaction $e^+e^- \to a^\pm b^\mp + e^+e^-$ via two-photon annihilation appears to be very small.

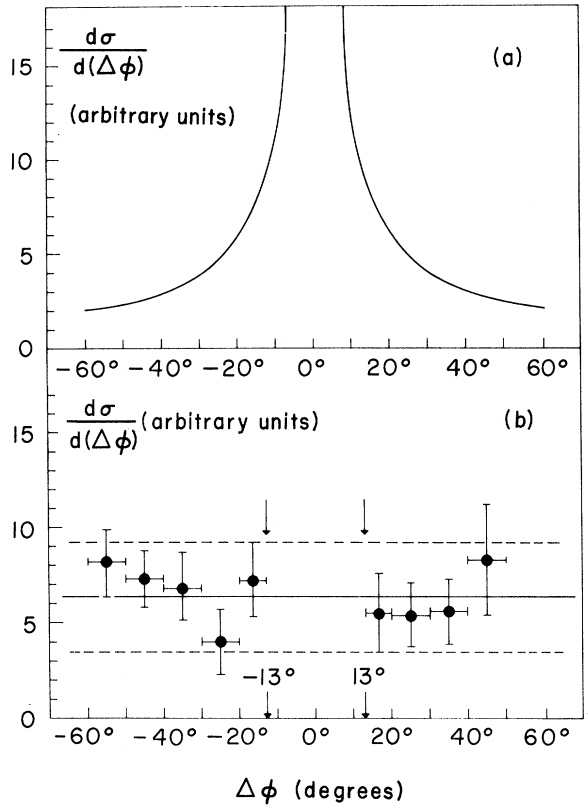

FIG. 15. (a) Theoretical shape of the differential cross section $d\sigma/d(\Delta\varphi)$ for the reaction $e^+e^- \to e^+e^-e^{+\prime}e^{-\prime}$, according to Baier and Fadin (Ref. 24); (b) $d\sigma/d(\Delta\varphi)$ calculated from the experimental $\Delta\varphi$ distribution of the two charged-track, 2τ, in-time, in-source noncoplanar events.

C. Data Corrections and Experimental Result

Several corrections must now be applied to the experimental data in order to obtain the total number of events which originate from the reaction $e^+e^- \to a^\pm + b^\pm$ + anything. First, many events with only two detected charged tracks (i.e., the detected configurations 2τ, $2\tau+\pi$, $2\tau+2\pi$) were rejected because of the noncoplanarity cut in $\Delta\varphi$. We recall that the noncoplanarity cut was set at 13° for events selected according to criterion (b) of Sec. V A (93% of the detected events with two charged tracks), while $|\Delta\varphi| \geq 40°$ was required for the events satisfying the selection criterion (c) (~7% of the total). The corresponding correction has been determined by a smooth interpolation between $-13° < \Delta\varphi < +13°$ ($-40° < \Delta\varphi < +40°$) of the experimental $\Delta\varphi$ distribution, which, we have seen, is

TABLE V. List of background-subtracted, in-time, in-source noncoplanar events according to their detected configuration, at the various energies, after the $\Delta\varphi$ cut correction has been applied. The raw numbers of collected events are given in parentheses (no events with four charged detected tracks have been found).

Total c.m. energy $E_+ + E_-$ (GeV)	Effective integrated luminosity (cm^{-2})	Corrected Bhabha events	Noncoplanar events					Total noncoplanar events
			$2\mathcal{T}$ events	$2\mathcal{T}+\mathcal{N}$ events	$2\mathcal{T}+2\mathcal{N}$ events	$3\mathcal{T}$ events	$3\mathcal{T}+\mathcal{N}$ events	
			(55)	(8)	(0)	(6)	(1)	(70)
1.4	119×10^{32}	472±33	40.6±9.4	6.4±3.5	0.0±1.1	5.4±2.5	0.6±1.1	53.0±10.4
			(100)	(15)	(1)	(12)	(1)	(128)
1.5	231	720±34	90.7±12.1	11.1±4.8	1.0±1.2	11.1±3.8	0.6±1.5	114.5±13.7
			(32)	(4)	(0)	(6)	(0)	(42)
1.6	67	166±17	26.5±7.0	2.3±2.4	0.0±1.1	5.3±2.5	0.0±1.1	34.6±7.9
			(44)	(7)	(2)	(2)	(2)	(57)
1.65	76	170±17	28.2±8.6	6.4±3.1	2.0±1.5	1.7±1.5	2.0±1.5	40.3±9.5
			(59)	(7)	(1)	(1)	(0)	(65)
1.7	130	261±21	42.9±9.7	4.1±3.3	0.3±1.1	0.0±1.2	0.0±1.3	47.3±10.5
			(46)	(4)	(0)	(4)	(0)	(54)
1.75	83	152±16	33.1±8.5	1.8±2.8	0.0±1.1	3.4±2.1	0.0±1.2	38.3±9.3
			(68)	(4)	(0)	(2)	(0)	(74)
1.8	115	189±18	50.1±10.5	1.0±2.6	−0.3±1.1	2.0±1.5	−0.3±1.3	52.5±11.0
			(110)	(23)	(2)	(10)	(2)	(146)
1.85	514	770±36	84.9±16.4	25.9±6.5	−2.0±1.5	10.6±4.2	2.7±2.3	122.1±18.6
			(45)	(3)	(2)	(3)	(0)	(53)
1.9	122	166±17	24.5±8.8	2.1±2.3	2.0±1.7	3.3±2.0	0.0±1.2	31.9±9.5
			(145)	(7)	(0)	(5)	(0)	(157)
2.0	257	293±25	90.4±17.9	5.8±3.7	0.0±1.1	5.8±2.7	−0.7±1.5	101.3±18.5
			(142)	(26)	(3)	(13)	(2)	(184)
2.4	751	453±23	22.6±24.6	21.9±6.3	3.9±2.5	12.7±4.1	1.7±2.0	62.8±25.9
			(846)	(108)	(11)	(64)	(8)	(1037)
Totals	2465×10^{32}	3812±83	534.5±43.7	89.3±13.6	6.9±4.0	61.3±9.1	6.6±5.0	698.6±47.1

consistent with a statistical angular distribution (see Sec. V B for reference). The over-all $\Delta\varphi$ cut correction to be applied to the 451 $2\mathcal{T}$ detected events was measured to be (+18±3)%; the correction to the 80 $2\mathcal{T}+\mathcal{N}$ detected events is (+12±4)%; and it is negligible for the $2\mathcal{T}+2\mathcal{N}$ configuration. Further corrections result from: losses due to the energy (range) cuts of the apparatus; nuclear interactions (absorption) of the produced particles; particles crossing the 22-cm Fe absorber and giving an anticoincidence signal pulse in the cosmic-ray veto counters; and, finally, multiple scattering. These corrections depend on the nature and the energy distribution of the emitted particles, i.e., on the particular physical channel through which the particles are produced. Therefore, these effects have been taken into account in the calculation of the detection efficiency of the apparatus performed with a Monte Carlo program according to each considered final state (see Appendix A).

Finally, the effect of the inefficiency of our monogap spark chambers has been included in the Monte Carlo calculation since also this correction depends on the actual final states produced.

The corrected numbers of events are listed in Table V for each c.m. energy, according to their different detected configurations. The only correction applied directly to the numbers of events is thus the $\Delta\varphi$ cut correction, all the other effects being taken into account in the efficiency calculation. Table V contains also, in parenthesis, the raw numbers of in-time, noncoplanar events coming from the source (4-chm + 3-chm events). In the third column of Table V we give the numbers of wide-angle Bhabha-scattering events simultaneously collected in our apparatus. These are the sum of 4-chm and 3-chm events (according to the definition of Sec. V A) and, after background subtractions, have been corrected for all the effects listed in Sec. IV C. Once the validity of QED has been established, the wide-angle Bhabha-scattering reaction can be used to determine the machine luminosity. This was done using the numbers of the third column of Table V. The effective cross section to detect in our apparatus 4- and 3-chm Bhabha events was computed by the Monte Carlo program.[26] The effective luminosities calculated in this way are listed in the second column of Table V. The determination of the luminosity from

the numbers of wide-angle Bhabha events detected by our apparatus is particularly convenient in order to evaluate absolute values of the cross sections for the reactions $e^+e^- \to a^\pm + a^\pm +$anything. In fact, this procedure minimizes effects due to the uncertainty in the actual value of the source length[9] and in the spark-chamber efficiency, which are in first approximation the same for the Bhabha and the noncoplanar events.[27]

In conclusion, the total number of events originating from the reaction $e^+e^- \to a^\pm + b^\pm +$anything detected by our apparatus with an integrated luminosity $\sim 2.5\times10^{35}$ cm^{-2} turns out to be 699. Since we have demonstrated that the produced particles are hadrons (the possible contamination of electrons being $<10\%$) in the following we will assume that they are pions, which is consistent with all our experimental information. Of course, we cannot exclude the possibility of kaon final states, especially at the higher center-of-mass energies.

D. Analysis of the Results and Absolute Values of the Cross Sections for the Reaction $e^+e^- \to a^\pm + b^\pm +$ Anything

The evaluation of cross sections from the experimental data requires the knowledge of the detection efficiency of our apparatus, which, of course, depends on the states actually produced.

The yield (n_D) of events in each detected configuration D ($D = 2\Upsilon$, $2\Upsilon+\mathfrak{N}$, $2\Upsilon+2\mathfrak{N}$, 3Υ, $3\Upsilon+\mathfrak{N}$, 4Υ) is related to the cross sections by the equation

$$n_D = \frac{N_D}{\mathcal{L}} = \sum_P \epsilon_D^P \sigma_P . \tag{5.3}$$

N_D is the total number of events detected in the configuration D; $\mathcal{L}$ is the integrated luminosity; σ_P is the cross section to produce a definite channel P (for example, P could be $e^+e^- \to \pi^+\pi^-\pi^0$, $e^+e^- \to \pi^+\pi^-\pi^+\pi^-$, etc.); and finally ϵ_D^P is the efficiency of our apparatus to detect the configuration D when the final particles are produced in channel P.

We have plotted in Figs. 16(a)–16(c) the experimental values of the yields for the statistically most significant detected configurations, i.e., 2Υ, $2\Upsilon+\mathfrak{N}$, and 3Υ. We have grouped the data into three energy bins, centered at 1.51, 1.82, and 2.3 GeV (weighted average). In Fig. 16(d) the total yield summed over all the detected configurations is also shown for each c.m. energy we have investigated. Finally in Fig. 17 we show that the energy dependence of the yield is the same for each of the detected configurations.

By using Eqs. (5.3) the prediction of any specific model, which provides the values of the σ_P's, can be easily compared with our n_D data, once the corresponding detection efficiencies ϵ_D^P have been calculated. As an example, we have drawn in Fig. 16 the predictions of some theoretical models,[28-30] using the efficiency values which are listed and discussed in Appendix A. The predictions of Layssac and Renard[29] result from a conventional one-photon approximation and assume vector-meson dominance of the electromagnetic interac-

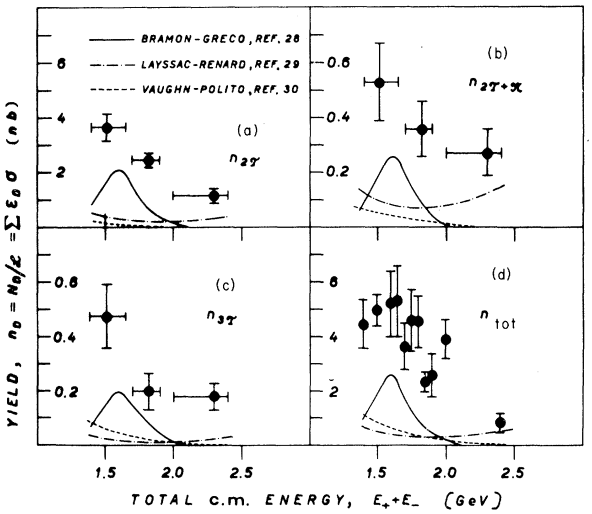

FIG. 16. Yield of noncoplanar corrected events. (a) Two charged tracks detected; (b) two charged tracks plus one neutral detected; (c) three charged tracks detected; (d) total yield (all the detected configurations). The curves are predictions of some theoretical models.

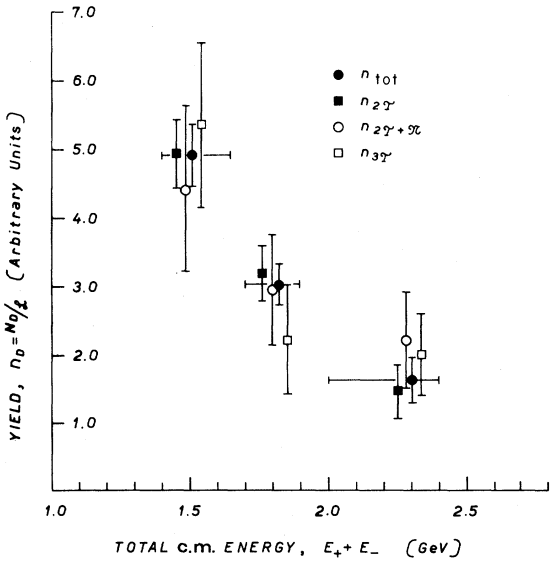

FIG. 17. Energy dependence of the yields. Different configuration yields are normalized to the same area.

tions to calculate multipion production from the high-energy tails of the ρ, ω, and ϕ mesons. The main contributions come from $A_1\pi$, $A_2\pi$, $\omega\pi$, and $\rho\rho$ production. Vaughn and Polito[30] have calculated the cross sections for the production of four charged pions through $A_1\pi, A_2\pi$ production. In both cases the predictions are much smaller than the experimental yields. The best prediction, in terms of absolute magnitude and energy dependence, is that of Bramon and Greco,[28] based on the existence of a heavy vector meson ρ' ($j^P = 1^-$, $I = 1$) whose parameters were deduced from the results of the SLAC streamer-chamber group on the reaction $\gamma + p \to p\pi^+\pi^-\pi^+\pi^-$.[31] But even in this case our experimental yields are at least a factor of 2 larger than the predictions.

Conversely, instead of comparing the theoretical to the experimental yields, we can attempt to solve the set of Eqs. (5.3) in terms of the unknown cross sections σ_P, once the detection efficiencies have been calculated. Let us first make a few comments on the detection efficiencies ϵ_D^P. As is discussed in Appendix A, for our experimental apparatus the calculated efficiencies are quite insensitive to the dynamics of the reaction, at least in the most reasonable cases we have considered, namely, statistical and quasi-two-body production (for any angular distribution of the type $A + B\sin^2\theta$). Therefore, the efficiencies used in the analysis are the ones calculated with the statistical model [invariant-phase-space (IPS) efficiencies]. Due to the small solid angle of the apparatus and the energy cuts on the detected particles, the values of the efficiencies are quite small, ranging from less than 1% to ~10% depending on the final state produced and the detected configuration. In our opinion this limits the quality of the results which can be obtained for the cross sections with all the existing small-solid-angle apparatus.

We can now proceed in the quantitative evaluation of the cross sections σ_P. We have six different detected configurations and therefore six equations (5.3). To these six equations we can add the following expression for the yield, N_M, of detected marked events (see Sec. V B for reference):

$$N_M = \sum_P f_M^P \epsilon^P \sigma_P . \tag{5.4}$$

The efficiencies $\epsilon_P = \sum_D \epsilon_P^D$ and the fractions of marked events due to the produced final-state P, f_M^P, are known from the Monte Carlo calculation (see Appendix A). In principle, this would allow us to extract from the data the cross sections for seven different channels P. However, only five of the seven equations are actually statistically significant. Moreover, the system of equations, (5.3) and (5.4), cannot be completely solved in terms of all the possible unknown σ_P's (whose number is limited only by energy conservation). Nevertheless some useful information can be extracted, under reasonably weak hypotheses, from our data. We have proceeded in the analysis as follows.

First we have restricted the possible σ_P's to the following six physical channels:

$$\sigma_{2\pi^\pm\pi^0} = \sigma(e^+e^- \to \pi^+\pi^-\pi^0),$$

$$\sigma_{2\pi^\pm 2\pi^0} = \sigma(e^+e^- \to \pi^+\pi^- 2\pi^0),$$

$$\sigma_{4\pi^\pm} = \sigma(e^+e^- \to \pi^+\pi^-\pi^+\pi^-),$$

$$\sigma_{4\pi^\pm\pi^0} = \sigma(e^+e^- \to \pi^+\pi^-\pi^+\pi^-\pi^0),$$

$$\sigma_{4\pi^\pm 2\pi^0} = \sigma(e^+e^- \to \pi^+\pi^-\pi^+\pi^- 2\pi^0),$$

$$\sigma_{6\pi^\pm} = \sigma(e^+e^- \to \pi^+\pi^-\pi^+\pi^-\pi^+\pi^-).$$

Numerical solutions of the equations in terms of the above unknown σ_P's have been tried. As is to be expected if one considers the values of the efficiencies (see Table VI, Appendix A), not all of the σ_P's can be well determined. In particular, the yields are practically independent of the ratios

$$y = \frac{\sigma(e^+e^- \to \pi^+\pi^-\pi^0}{\sigma(e^+e^- \to \pi^+\pi^- 2\pi^0)}$$

and

$$z = \frac{\sigma(e^+e^- \to \pi^+\pi^-\pi^+\pi^-\pi^0)}{\sigma(e^+e^- \to \pi^+\pi^-\pi^+\pi^- 2\pi^0)} .$$

In addition, since the detection efficiencies for the reactions $e^+e^- \to \pi^+\pi^-\pi^0$ and $e^+e^- \to \pi^+\pi^- 2\pi^0$ are quite small, our counting rates are also not very sensitive to the magnitude of $\sigma(e^+e^- \to \pi^+\pi^-\pi^0)$ and $\sigma(e^+e^- \to \pi^+\pi^- 2\pi^0)$.

Therefore, we have found it convenient to express our results in terms of the following independent combinations of the σ_P's:

$$\sigma_{\text{tot}} = \sigma_{2\pi^\pm\pi^0} + \sigma_{2\pi^\pm 2\pi^0} + \sigma_{4\pi^\pm} + \sigma_{4\pi^\pm\pi^0} + \sigma_{4\pi^\pm 2\pi^0} + \sigma_{6\pi^\pm},$$

$$\sigma_C = \sigma_{4\pi^\pm} + \sigma_{6\pi^\pm},$$

$$\sigma_{4\pi^\pm},$$

$$x = \frac{\sigma_{2\pi^\pm\pi^0} + \sigma_{2\pi^\pm 2\pi^0}}{\sigma_{4\pi^\pm} + \sigma_{4\pi^\pm\pi^0} + \sigma_{4\pi^\pm 2\pi^0} + \sigma_{6\pi^\pm}} = \frac{\sigma_{2\pi^\pm, N}}{\sigma_{\geq 4\pi^\pm, \text{tot}}},$$

$$y = \frac{\sigma_{2\pi^\pm\pi^0}}{\sigma_{2\pi^\pm 2\pi^0}},$$

$$z = \frac{\sigma_{4\pi^\pm\pi^0}}{\sigma_{4\pi^\pm 2\pi^0}},$$

and we have solved the system of Eqs. (5.3) and

TABLE VI. Values of the statistical efficiencies of our apparatus for each detected configuration, for several possible produced final states of pions, at three different values of the total c.m. energy, $E_+ + E_-$. Invariant phase-space distribution of the produced particles was assumed.

Produced final state	$E_+ + E_-$ (GeV)	Efficiency for detection of $2T$ (%)	$2T+1N$ (%)	$2T+2N$ (%)	$3T$ (%)	$3T+1N$ (%)	$4T$ (%)
$\pi^+\pi^-\pi^0$	1.4	2.2	0.7	0.0			
	1.8	1.4	0.5	0.0			
	2.4	0.6	0.2	0.0			
$\pi^+\pi^-2\pi^0$	1.4	1.1	0.7	0.2			
	1.8	1.0	0.7	0.1			
	2.4	0.7	0.4	0.1			
$\pi^+\pi^-3\pi^0$	1.4	0.5	0.4	0.2			
	1.8	0.6	0.5	0.2			
	2.4	0.6	0.3	0.2			
$\pi^+\pi^-4\pi^0$	1.4	0.1	0.2	0.1			
	1.8	0.2	0.4	0.2			
	2.4	0.2	0.3	0.2			
$\pi^+\pi^-\pi^+\pi^-$	1.4	8.5			0.9		0.0
	1.8	7.0			0.7		0.0
	2.4	4.0			0.4		0.0
$\pi^+\pi^-\pi^+\pi^-\pi^0$	1.4	4.0	1.5	0.0	0.4	0.1	0.0
	1.8	4.1	1.4	0.0	0.4	0.1	0.0
	2.4	3.5	1.0	0.0	0.2	0.1	0.0
$\pi^+\pi^-\pi^+\pi^-2\pi^0$	1.4	1.6	1.0	0.1	0.1	0.1	0.0
	1.8	2.4	1.7	0.4	0.3	0.1	0.0
	2.4	2.0	1.4	0.3	0.2	0.2	0.0
$3\pi^-3\pi^+$	1.4	6.5			0.6		0.0
	1.8	8.8			1.3		0.1
	2.4	7.4			1.1		0.1
$4\pi^+4\pi^-$	1.4	0.1			0.0		0.0
	1.8	6.3			0.7		0.0
	2.4	8.3			1.8		0.1

(5.4) with x, y, and z as free parameters. For each value of x, we find that σ_{tot}, σ_C, and $\sigma_{4\pi^\pm}$ are rather well determined while they are not affected very much by the values assigned to the parameters y and z (on which the equations are practically independent). As an example, we show in Fig. 18 the values of σ_{tot} and σ_C, as a function of x for the three averaged energies 1.51 GeV, 1.82 GeV, and 2.30 GeV. The dashed bands indicate, for each value of x, the range of solutions obtained by varying y and z from zero to infinity. The white bands represent the statistical uncertainty. No acceptable solutions were found for values of $x \gtrsim 3$ at 1.51 GeV, and $x \gtrsim 5$ at 1.82 and 2.30 GeV.[32]

If we restrict the value of x to the region $0.2 \leq x \leq 2$, then σ_{tot}, σ_C, and $\sigma_{4\pi^\pm}$ are determined as shown in Figs. 19(a), 19(b), and 20(a). Moreover, from σ_{tot}, σ_C, and $\sigma_{4\pi^\pm}$ we can extract $\sigma_{6\pi^\pm}$ and, with larger errors, $\sigma_{4\pi^\pm,N}$ as shown in Figs. 20(b) and 20(c). The interval of x chosen is conservatively large. In fact, the ratio $\sigma_{2\pi^\pm,N}/\sigma_{\geq 4\pi^\pm,\text{tot}}$ is always ≥ 0.2 for any possible isotopic-spin configuration,[33] thus setting the lower limit for x. On the other hand, a value of x larger than two is strongly inconsistent with the results of all the other Adone groups.[34]

Finally in Fig. 21 we compare our experimental data (i.e., the yields for each different detected configuration, the fraction of marked events and the $\Delta\varphi$ distribution) with the results obtained, using the admixture of final states indicated by the best-fit procedure, from the IPS Monte Carlo program (see Appendix A). The general agreement is quite satisfactory, the only discrepant experimental point being the fraction of marked events at 1.51 GeV which we have already discussed in Ref. 32.

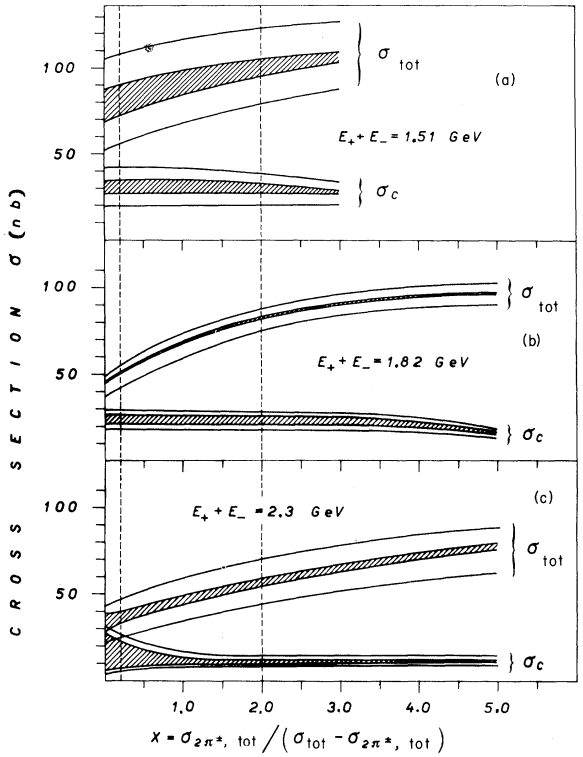

FIG. 18. Reactions $e^+e^- \to a^\pm + b^\pm$ + anything. The total cross section, σ_{tot}, and $\sigma_c = \sigma_{4\pi^\pm} + \sigma_{6\pi^\pm}$ are given as functions of the parameter

$$x = \frac{\sigma_{2\pi^\pm\pi^0} + \sigma_{2\pi^\pm 2\pi^0}}{\sigma_{4\pi^\pm} + \sigma_{4\pi^\pm\pi^0} + \sigma_{4\pi^\pm 2\pi^0} + \sigma_{6\pi^\pm}} .$$

Dashed bands indicate the range covered by σ_{tot} and σ_c when the parameters $y = \sigma_{2\pi^\pm\pi^0}/\sigma_{2\pi^\pm 2\pi^0}$ and $z = \sigma_{4\pi^\pm\pi^0}/\sigma_{4\pi^\pm 2\pi^0}$ vary from zero to infinity, while the outer bands show the statistical uncertainty. (a) $E_+ + E_- = 1.51$ GeV; (b) $E_+ + E_- = 1.82$ GeV; (c) $E_+ + E_- = 2.30$ GeV.

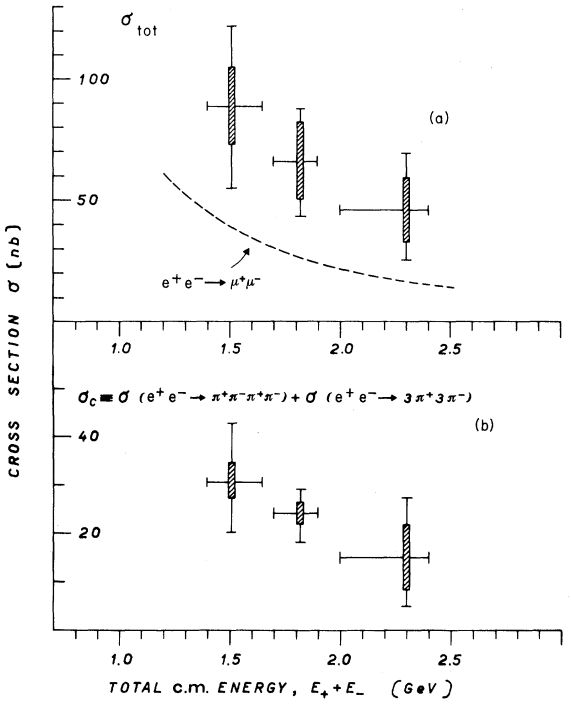

FIG. 19. Reactions $e^+e^- \to a^\pm + b^\pm$ + anything. Values of the cross sections are given for $0.2 \le x \le 2$. For each point the dashed rectangles indicate the range of values obtained varying y and z from zero to infinity, while the statistical errors are shown as bars. (a) Total cross section, σ_{tot}; for reference, the total cross section to produce a pair of μ mesons is also plotted; (b) cross section for totally charged produced particles, $\sigma_c = \sigma_{4\pi^\pm} + \sigma_{6\pi^\pm}$.

E. Conclusions

We can summarize the experimental information on the reaction $e^+e^- \to a^\pm + b^\pm$ + anything as follows:

(a) We have collected 605 events originated from the above reaction, at c.m. energies between 1.4 and 2.4 GeV, for a total integrated luminosity $\mathcal{L} \simeq 2.5 \times 10^{35}$ cm^{-2}.

(b) $a^\pm$ and $b^\pm$ appear to be hadrons, the possible contamination from electrons being demonstrated to be less than ~10%. In particular, the total possible contamination from reactions of the type $e^+e^- \to e^+ + e^-$ + anything via a two-photon-interaction channel[24,25] is negligible (<10%) in the noncoplanarity region investigated ($|\Delta\varphi| \ge 13°$).

(c) The total cross section for reaction $e^+e^- \to a^\pm + b^\pm$ + anything has been determined. The obtained values turn out to be surprisingly large,[7] ranging from 50 to 90 nb, in the energy interval 1.4 to 2.4 GeV. The cross sections for some particular final states ($e^+e^- \to \pi^+\pi^-\pi^+\pi^-$, $e^+e^- \to \pi^+\pi^-\pi^+\pi^-$ + neutrals, $e^+e^- \to \pi^+\pi^-\pi^+\pi^-\pi^+\pi^-$) have also been determined.

In Figs. 22 and 23 our results are compared with those of other storage-ring experiments.[35-38] The total cross section is shown in Fig. 22(c). There appears to be a rather striking increase of σ_{tot} between 1.0 and 1.5 GeV, followed by a slow falloff, consistent with a $1/E^2$ dependence. In Figs. 22(a), 22(b), and 23, the cross sections for some particular channels are also plotted. The energy dependence appears to be quite different for the various channels. In particular, the cross section for the reaction $e^+e^- \to \pi^+\pi^-\pi^+\pi^-$ [Fig. 22(a)] shows a peculiar behavior: It rises sharply from less than 2 nb at 0.99 GeV up to ~30 nb at ~1.5 GeV, and then falls off to less than ~5 nb at 2.0–2.4 GeV. This behavior could possibly be explained by a resonant production mechanism (ρ') as discussed in Ref. 28.

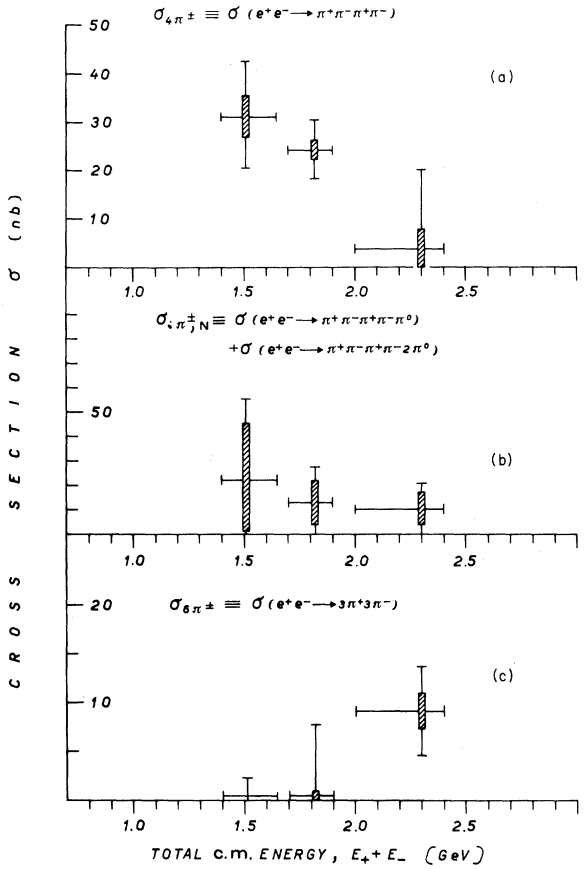

FIG. 20. Reactions $e^+e^- \to a^\pm + b^\pm$ + anything. Values of the cross sections are given for $0.2 \leq x \leq 2$. For each point the dashed rectangles indicate the range of values obtained varying y and z from zero to infinity, while the statistical errors are shown as bars. (a) Cross section to produce four charged pions $\sigma_{4\pi^\pm}$; (b) cross section to produce four charged pions plus neutrals, $\sigma_{4\pi^\pm,N}$; (c) cross section to produce six charged pions, $\sigma_{6\pi^\pm}$.

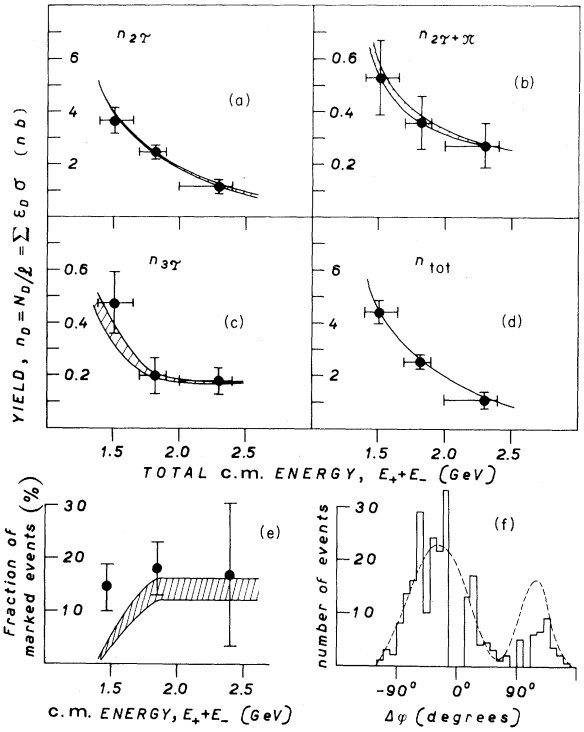

FIG. 21. Comparison of the experimental data on the reactions $e^+e^- \to a^\pm + b^\pm$ + anything with the results of the fit (shown as curves and dashed bands in the figure). (a) Yield of two charged detected tracks events; (b) yield of two charged plus one neutral detected tracks events; (c) yield of three charged detected tracks events; (d) total yield (all the detected configurations); (e) fraction of marked events; (f) $\Delta\varphi$ distribution of two charged track events (4-chm events).

ACKNOWLEDGMENTS

We wish to thank the many people who worked in the early stages of this experiment: B. Coluzzi, G. Goggi, F. Massa, D. Scannicchio, and N. Spinelli, and, in particular, C. Bernardini for having stimulated this experiment and for continuous encouragement and useful discussion. Our technician G. Schina made a valuable contribution to the setting up and maintenance of the apparatus. The monitor group made available to us their luminosity measurements. Finally we thank the Adone staff for their cooperation, Dr. A. Rambaldi for considerable assistance in the computer analysis, and all the members of the other Adone groups for many discussions.

APPENDIX A: THE MONTE CARLO CALCULATION

In order to understand the response of our experimental apparatus to the reactions which were the object of our experimental study (i.e., elastic electron-positron scattering and production of multihadron states), a Monte Carlo calculation has been performed. This calculation takes into account, in addition to the geometrical features of the apparatus, also the energy cuts (range), the nuclear absorption (see Appendix B), the efficiency of the spark chambers, and the effects of the extended source (see Ref. 9, Sec. II). It also takes into account the possibility of a misidentification of the tracks due to the presence of more than one particle in a chamber since we can identify only one track per chamber. For the elastic electron-positron scattering we have made use of the Bhabha cross section. For the multihadron processes several different models have been used. We report in this appendix the results which are of inter-

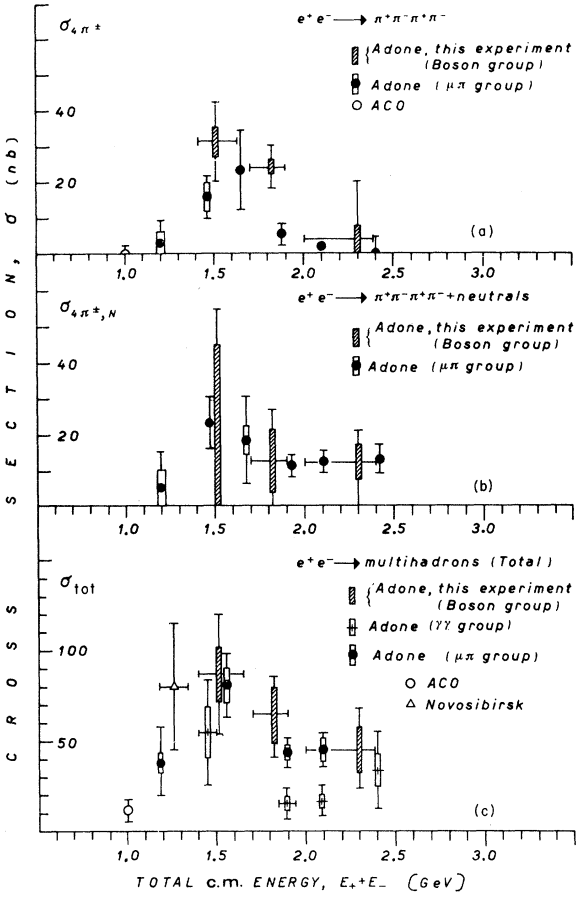

FIG. 22. Summary of the experimental determination of the cross sections for reactions $e^+e^- \rightarrow a^\pm + b^\pm +$ anything. Our results are compared with the data from ACO (Ref. 35), Novosibirsk (Ref. 36), the Adone $\gamma\gamma$ Group (Ref. 37), and the Adone $\mu\pi$ Group (Ref. 38). Systematic uncertainties are indicated as rectangles. (a) Cross section to produce four charged pions, $\sigma_{4\pi^\pm}$; (b) cross section to produce four charged pions plus neutrals, $\sigma_{4\pi^\pm,N}$; (c) total cross section σ_{tot}.

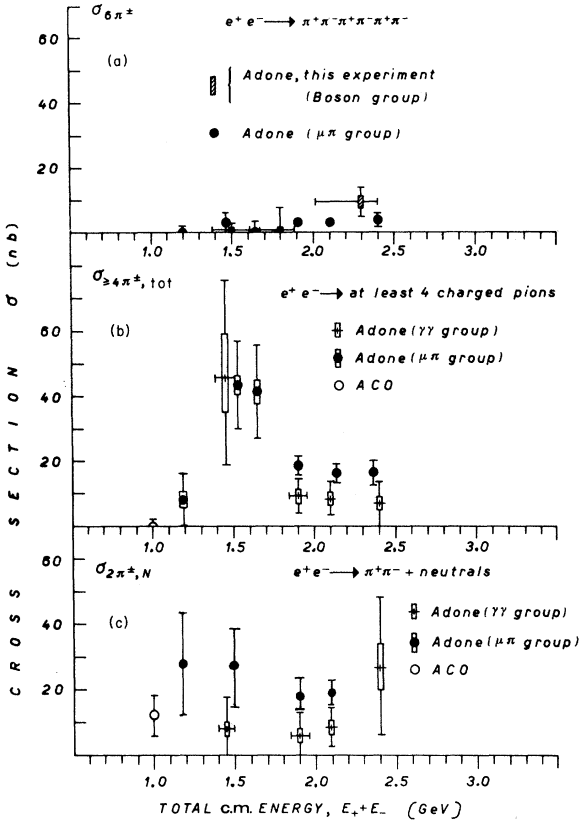

FIG. 23. Summary of the experimental determinations of the cross sections for reactions $e^+e^- \rightarrow a^\pm + b^\pm +$ anything. Our results are compared with the data from ACO (Ref. 35), the Adone $\gamma\gamma$ Group (Ref. 37), and the Adone $\mu\pi$ Group (Ref. 38). Systematic uncertainties are indicated as rectangles. (a) Cross section to produce six charged pions $\sigma_{6\pi^\pm}$; (b) cross sections to produce at least four charged pions (plus possible neutrals), $\sigma_{4\pi^\pm,tot}$; (c) cross sections to produce two charged pions plus neutrals, $\sigma_{2\pi^\pm,N}$.

est for the interpretation of our data.

First, in Table VI we list at three different c.m. energies the values of the detection efficiencies which were used for the analysis of our experimental data. They refer to the processes

$$e^+e^- \rightarrow n\pi^+ + n\pi^- + m\pi^0 .$$

Angular and energy distributions have been calculated in the frame of the statistical model (IPS distributions).

To give a quantitative feeling of how much the different effects involved affect the values of the efficiencies, we refer, as a typical example, to the efficiency $\epsilon_{2\tau}^{4\pi^\pm}$ to detect a two-charged configuration (2τ) from the reaction $e^+e^- \rightarrow \pi^+\pi^-\pi^+\pi^-$, calculated at total c.m. energy $E_+ + E_- = 1.8$ GeV.

In this case the geometrical efficiency, for a point-like interaction region, is ~29%, and it is reduced to ~14.5% when one takes into account the effective length of the source (see Ref. 9). Including the low-energy cut (determined by the amount of absorber before the trigger counters) further reduces ϵ to 13%, while the upper-energy cut lowers it to 8%. The effect of switching on nuclear interactions is to raise ϵ to ~9%. Including the spark-chamber inefficiencies gives the effective detection efficiency quoted in Table VI, i.e., $\epsilon = 7\%$. The relatively small effect of the nuclear interactions (which appear to produce a net variation of ~10% in the value of the efficiency) is the result of a partial cancellation: in fact, while turning on nuclear interactions increases losses in the absorbers before the trigger counters, at the same time it reduces from 40% to ~10% the fraction of events in

TABLE VII. Values of the efficiencies of our apparatus for each particular detected configuration from four-pion final states, produced via a quasi-two-body intermediate state.

Produced final state	$E_+ + E_-$ (GeV)	Efficiency for detection of $2\mathcal{T}$ (%)	$2\mathcal{T}+1\mathcal{N}$ (%)	$2\mathcal{T}+2\mathcal{N}$ (%)	$3\mathcal{T}$ (%)	$3\mathcal{T}+1\mathcal{N}$ (%)	$4\mathcal{T}$ (%)
$\omega\pi^0 \to \pi^+\pi^- 2\pi^0$	1.4	0.5	0.4	0.1			
	1.8	0.4	0.2	0.0			
	2.4	0.3	0.2	0.1			
$A_1^\pm \pi^\mp \to \pi^+\pi^- 2\pi^0$	1.4	1.0	0.6	0.2			
	1.8	1.1	0.7	0.1			
	2.4	0.6	0.4	0.0			
$A_2^\pm \pi^\mp \to \pi^+\pi^- 2\pi^0$	1.4	0.4	0.3	0.1			
	1.8	1.0	0.5	0.1			
	2.4	0.5	0.4	0.1			
$A_1^\pm \pi^\mp \to \pi^+\pi^-\pi^+\pi^-$	1.4	8.9			0.9		0.0
	1.8	7.3			0.6		0.0
	2.4	3.6			0.4		0.0
$A_2^\pm \pi^\mp \to \pi^+\pi^-\pi^+\pi^-$	1.4	7.7			0.6		0.0
	1.8	7.3			0.6		0.1
	2.4	4.1			0.5		0.0

which a particle crossing the iron roof absorber is vetoed by the cosmic-ray counters.

Finally, it is interesting to recall (see Sec. VC) that we have used the rate of the wide-angle e^+e^- elastic scattering events collected in our apparatus as a luminosity monitor for the hadronic events. The fact that we have computed the detection efficiency for e^+e^- pair with the same Monte Carlo distribution minimizes the effects on the cross sections of uncertainties in the actual values of the source length and of the spark-chambers efficiencies.

In Table VII we give for comparison the values of the detection efficiencies for 4-pion final states, calculated with different dynamical models, via quasi-two-body intermediate states, namely,

$$e^+e^- \to A_1^\pm \pi^\mp \begin{cases} \pi^+\pi^-\pi^0\pi^0 \\ \pi^+\pi^-\pi^+\pi^- \end{cases},$$

$$e^+e^- \to A_2^\pm \pi^\mp \begin{cases} \pi^+\pi^-\pi^0\pi^0 \\ \pi^+\pi^-\pi^+\pi^- \end{cases},$$

$$e^+e^- \to \omega\pi^0 \to \pi^+\pi^-\pi^0\pi^0 .$$

The intermediate particles (A_1, A_2, ω) have been

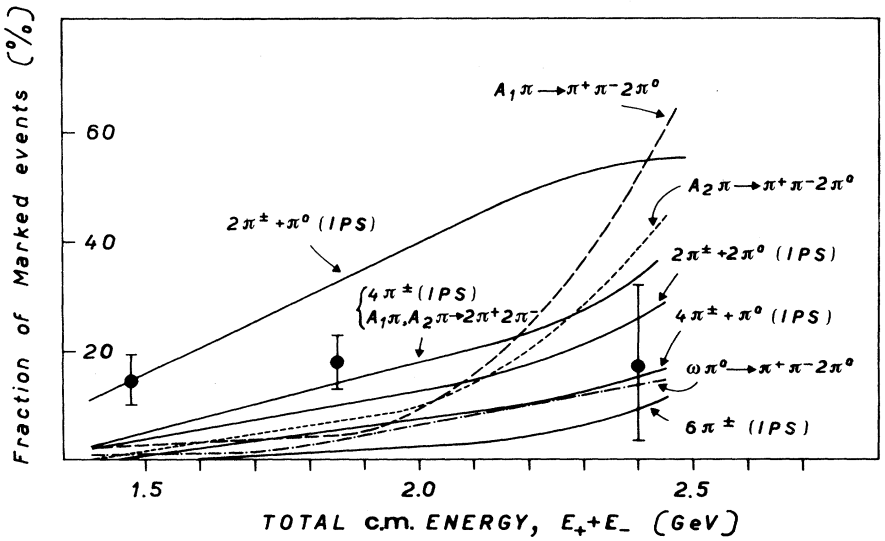

FIG. 24. Fraction of marked events, f_M, calculated with the Monte Carlo program for several different processes, compared with the experimental values for the reactions $e^+e^- \to a^\pm + b^\pm +$ anything.

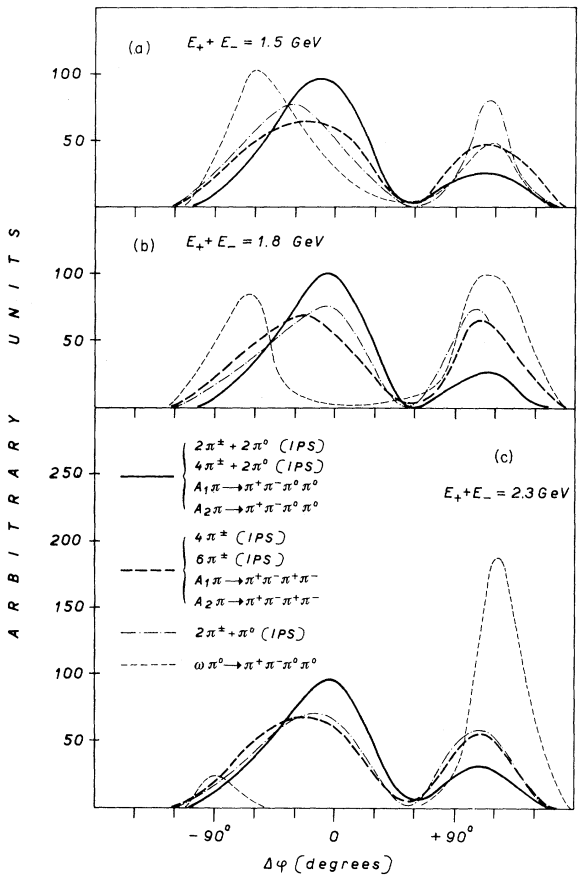

FIG. 25. $\Delta\varphi$ distribution for the configuration 2τ, calculated with the Monte Carlo program for several different processes. (a) $E_+ + E_- = 1.5$ GeV; (b) $E_+ + E_- = 1.8$ GeV; (c) $E_+ + E_- = 2.3$ GeV.

assumed to decay isotropically and to be statistically produced. We have checked that a production distribution of the type $A + B\sin^2\theta$, because of the extension of the source, does not appreciably affect the values of the efficiencies (few percent variations), irrespective of the values chosen for A and B. It can be seen from Table VII that the efficiencies for these quasi-two-body channels do not differ, apart from threshold effects, from the corresponding statistical efficiencies (Table VI) by more than 10–20%; the only exception being the case $e^+e^- \to \omega\pi^0$, whose detection efficiency is twice as small as for the corresponding statistical channel $e^+e^- \to \pi^+\pi^-\pi^0\pi^0$. It is worthwhile to note that the values of cross sections obtained from our experimental data, using the efficiencies of either Tables VI or VII, turn out to be the same within the statistical errors.

In Fig. 24 we show as a function of the c.m. energy the fraction, f_M, of events which, according to the Monte Carlo calculation, are expected to be marked. For reference, we have also plotted in the same figure the experimental values of f_M (see Sec. V B).

Finally, in Fig. 25 the $\Delta\varphi$ distributions calculated with the Monte Carlo program for several different channels are shown. Figure 25(a) refers to $E_+ + E_- = 1.5$ GeV while Figs. 25(b) and 25(c) refer to 1.8 and 2.3 GeV, respectively. Apart from the $e^+e^- \to \omega\pi^0$ and $e^+e^- \to \pi^+\pi^-\pi^0$ (IPS channels, which show a peculiar behavior, the $\Delta\varphi$ distributions of all the other channels can be grouped in the two different typical distribution shown in Fig. 25.

TABLE VIII. List of materials and corresponding thicknesses, t, of one of the top telescopes (the bottom telescopes end after counter D_i).

Material	Thickness, t (g/cm^2)
Fe (vacuum chamber walls)	1.2
Glass (wire chamber $SC\alpha_i$)	1.1
Scintillator (counter A_i)	2.0
Al	5.2
Scintillator (counter B_i)	1.4
Al	1.7
Glass (wire chamber $SC\beta_i$)	1.1
Pb	8.0
Fe	1.6
Scintillator (counter C_i)	2.8
Fe	1.6
Pb	8.0
Fe	1.6
Scintillator (counter D_i)	2.8
Fe	1.6
Al	2.4
Fe (22 cm)	158.0
Scintillator [counter CR_1 (CR_2)]	3.2
Fe (1.5 cm)	19.0
Pb (5 cm)	56.7
Scintillator [counter CR_3 (CR_4)]	2.7

APPENDIX B: ABSORPTION AND SECONDARY-PARTICLE PRODUCTION

1. Absorption and Secondary-Particle Production

We wish to calculate the fraction of an incident pion beam which enters a downstream counter after traversing a series of consecutive absorbers at an angle ψ with respect to the absorber surfaces. Table VIII lists the constituents of one of the telescopes of our experimental apparatus, and their thickness t_i.

First, considering the absorption of the primary beam, if N_0 is the initial number of pions, then

$$N_{1,\mathrm{pr}} = N_0 \exp[-x_1/\langle\lambda_{1,\mathrm{abs}}(E_{\pi,1})\rangle_{\mathrm{av}}] \qquad \text{(B1)}$$

is the number of pions remaining after the first

absorber. x_1 is the path length ($x_1 = t_1/\cos\psi$) and $\lambda_{1,\mathrm{abs}}(E_{\pi,1})$ is the absorption length for the pion to have any inelastic interaction, independent of the number of secondary particles produced. $\lambda_{1,\mathrm{abs}}(E_{\pi,1})$ is a function of the pion energy and $\langle\lambda_{1,\mathrm{abs}}(E_{\pi,1})\rangle_{\mathrm{av}}$ is the average value over the absorber x_1. As we will see, $\lambda_{\mathrm{abs}}(E_\pi)$ is approximately constant above ~300 MeV, so we will not write the energy dependence explicitly in the remaining expressions of this section. Clearly, the expression for the number ($N_{\mathrm{tot,pr}}$) of pions remaining after a series of n absorbers is

$$N_{\mathrm{tot,pr}} = N_0 \exp\left(-\sum_{i=1}^{n} \frac{x_i}{\lambda_{i,\mathrm{abs}}}\right). \tag{B2}$$

To begin the calculation of secondary-particle production, we write, for a given absorber of thickness T, the probability for a primary pion entering the absorber to produce a secondary between x and dx (with an energy, E_{sec}, greater than E_m, into a solid angle $\Delta\Omega$) as

$$P(x)dx = e^{-x/\lambda_{\mathrm{abs}}} \frac{dx}{\lambda_{\mathrm{abs}}} p(E_\pi, E_m),$$

where $e^{-x/\lambda_{\mathrm{abs}}}$ is the fraction of pions remaining at the point x, $dx/\lambda_{\mathrm{abs}}$ is the probability of interaction in dx, and $p(E_\pi, E_m)$ is the probability to produce a secondary (once a primary pion has been absorbed) within a solid angle $\Delta\Omega$ (for instance, the solid angle subtended by a downstream counter placed after the absorber T), with a certain minimum energy E_m (for instance, the minimum energy necessary to emerge from T). Moreover, the probability that the secondary pions remain (are not absorbed) after they pass through the remaining $(T-x)$ absorber is

$$\frac{1}{\Delta\Omega}\int_{\Delta\Omega} e^{-(T-x)/(\lambda_{\mathrm{abs}}\cos\psi_s)}\, d\Omega \equiv f(x) e^{-(T-x)/\lambda_{\mathrm{abs}}},$$

where the angular average has been taken into account by the function $f(x)$. So, integrating through the whole absorber, we can write for the number (N_{sec}) of secondary particles entering a downstream counter after traversing an absorber of thickness T

$$N_{\mathrm{sec}} = N_0 (e^{-T/\lambda_{\mathrm{abs}}}) \frac{T}{\lambda_{\mathrm{abs}}} \langle p(E_\pi, E_m) f(x)\rangle_{\mathrm{av}}. \tag{B3}$$

N_0 is the number of incident pions and $\langle p(E_\pi, E_m) f(x)\rangle_{\mathrm{av}}$ is the average of $p(E_\pi, E_m) f(x)$ over the whole absorber T.

We can now proceed with the calculation for n absorbers by noticing that, for instance, the number of secondaries that are produced by primary pions in the second absorber of thickness x_2 and appear after the nth absorber is

$$N_{2,\mathrm{sec}} = (N_0 e^{-x_1/\lambda_{1,\mathrm{abs}}})(e^{-x_2/\lambda_{2,\mathrm{abs}}}) \frac{x_2}{\lambda_{2,\mathrm{abs}}} \langle p_2(E_{\pi,2}, E_{m,2}) f_2\rangle_{\mathrm{av}} \left[\exp\left(-\sum_{i=3}^{n} \frac{x_i}{\lambda_{i,\mathrm{abs}}}\right)\right].$$

We have not considered additional pion production by the secondaries themselves since the secondaries have only a small fraction of the incident energy and the secondary production cross section is shown to be very small below 300 MeV [see Fig. 27(a)]. So, summing the secondaries from all n absorbers, we have

$$N_{\mathrm{tot,sec}} = N_0 \sum_{i=1}^{n} \frac{x_i \langle p_i(E_{\pi,i}, E_{m,i}) f_i\rangle_{\mathrm{av}}}{\lambda_{i,\mathrm{abs}}} \left[\exp\left(-\sum_{i=1}^{n} \frac{x_i}{\lambda_{i,\mathrm{abs}}}\right)\right]. \tag{B4}$$

By summing Eqs. (B2) and (B4), the total number (N_{tot}) of pions entering a downstream counter after traversing a set of n absorbers is given by

$$N_{\mathrm{tot}} = N_{\mathrm{tot,pr}} + N_{\mathrm{tot,sec}} = N_0 \left[\exp\left(-\sum_{i=1}^{n} \frac{x_i}{\lambda_{i,\mathrm{abs}}}\right)\right]\left(1 + \sum_{i=1}^{n} \frac{x_i \langle p_i(E_{\pi,i}, E_{m,i}) f_i\rangle_{\mathrm{av}}}{\lambda_{i,\mathrm{abs}}}\right). \tag{B5}$$

2. Measurements of Absorption Cross Section and Secondary-Particle Production Cross Section

The absorption cross section (σ_{abs}) and secondary-particle cross section (σ_{sec}) have been experimentally determined by several groups.[39-43] In general, we have made use only of those counter experiment data that conform mostly to our experimental set up. "Good geometry" measurements[39,40] permit a determination of σ_{abs} and σ_{sec} by fitting the solid-angle dependence of the experimental results, assuming that

$$\sigma_{\mathrm{exp}}(\Delta\Omega) = \sigma_{\mathrm{diff}}(\Delta\Omega) + \sigma_{\mathrm{abs}} - \sigma_{\mathrm{sec}}(\Delta\Omega). \tag{B6}$$

$d\sigma_{\mathrm{sec}}/d\Omega$ was assumed to be isotropically distributed, and $\sigma_{\mathrm{diff}}(\Delta\Omega)$ (the elastic scattering cross section) was calculated using an optical model.

For each of the references (39–43) the values of σ_{abs} determined for different elements from the

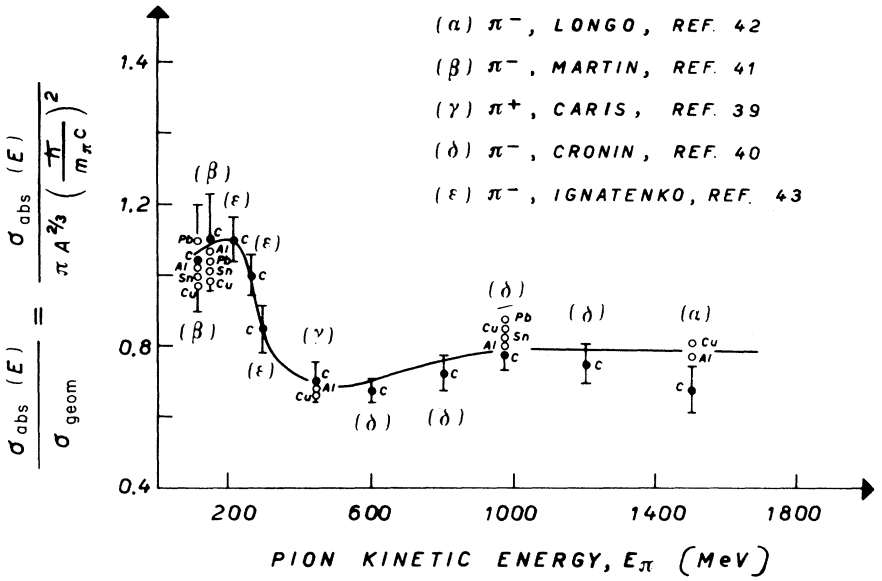

FIG. 26. Ratio $R(E_\pi)=\sigma_{abs}/\sigma_{geom}$ as a function of the pion kinetic energy E_π.

experiments are shown in Fig. 26 as a function of the pion kinetic energy, E_π. These values of σ_{abs} have been divided by $\sigma_{geom}=\pi A^{2/3}(\hbar/m_\pi c)^2$. The graph indicates that within the errors at each energy the ratio of the absorption to geometrical cross section is the same for all elements. This allows one to write a single energy dependence of $\sigma_{abs}/\sigma_{geom}$ for all elements. The energy dependence shows the effect of the (3, 3) resonance near E_π = 200 MeV, but is almost constant ($\sigma_{abs}/\sigma_{geom}\sim 0.7$) at higher energies [consistent with the usual convention $\sigma_{abs}=(\frac{2}{3})\sigma_{geom}$]. We define for further use $R(E_\pi)=\sigma_{abs}(E_\pi)/\sigma_{geom}$.

From Refs. 39, 40, and 43, the Figs. 27(a) and 27(b) show the energy and atomic weight (A) dependence of $\sigma_{sec}(\Delta\Omega)$ determined from fits to $\sigma_{exp}(\Delta\Omega)$. For the secondary-particle cross section a form $d\sigma_{sec}=\eta d\Omega$ was assumed, that is, an isotropic production of secondaries. As can be seen, secondary-particle production is quite small below 200 MeV but rises linearly with incident pion energy. By using the curves in Figs. 27(a) and 27(b) η [and therefore $\sigma_{sec}(\Delta\Omega)$] can be determined for any type of absorber and any pion energy. In addition, measurements of the energy distributions of secondaries has been carried out in several experiments.[43] Figure 28 shows the results of these measurements plotted in a useful manner. For any fraction, E/E_π, of the incident pion energy (E_π) the graph indicates directly the probability that the secondary energy is greater than E. The dashed line in Fig. 28 is an average used in the calculation.

All of these experimental determinations assume

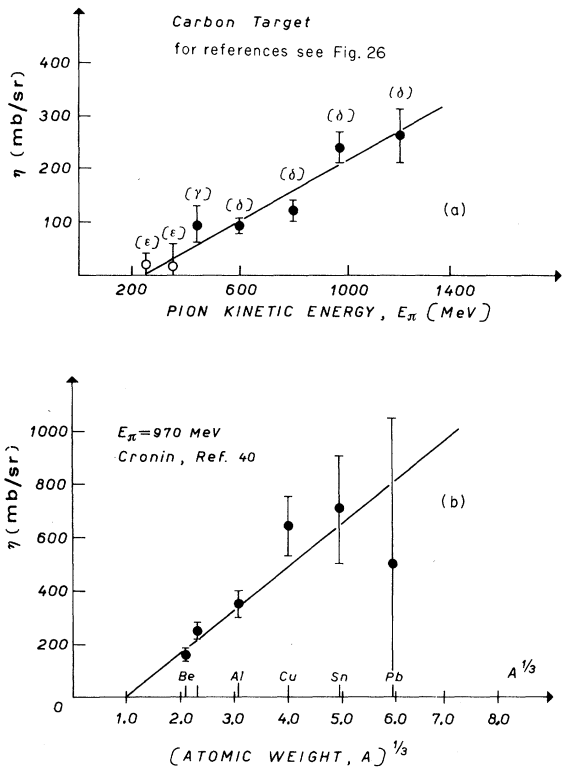

FIG. 27. Cross sections for secondary-particle production. (a) η as a function of the incident pion kinetic energy for a carbon target; (b) η as a function of the atomic weight, A, for an incident pion kinetic energy $E_\pi=970$ MeV.

that the total number of pions emerging from an absorber of thickness T (after the diffractive scattering component is subtracted) is given by

$$N_{\rm tot}=N_0 e^{-T/\langle\lambda_{\rm abs}\rangle_{\rm av}}\{\exp[T\langle\sigma_{\rm sec}(\Delta\Omega)\rangle_{\rm av}\mathfrak{N}_A/A]\}, \tag{B7}$$

where $\langle\sigma_{\rm sec}(\Delta\Omega)\rangle_{\rm av}=\langle\eta\Delta\Omega\rangle_{\rm av}$ (the average being performed over the whole absorber), $\mathfrak{N}_A$ is Avogadro's number, and A is the atomic weight of the absorber. Using our previous notation, and summing the equations (B1) (for $x_1=T$) and (B3), we write

$$N_{\rm tot}=N_{\rm pr}+N_{\rm sec}$$
$$=N_0 e^{-T/\lambda_{\rm abs}}\left(1+\frac{T}{\lambda_{\rm abs}}\langle p(E_\pi,E_m)f\rangle_{\rm av}\right). \tag{B8}$$

Then by comparing Eq. (B7) with Eq. (B8) we can make the following identification:

$$\frac{T}{\lambda_{\rm abs}}\langle p(E_\pi,E_m)f\rangle_{\rm av}\to\frac{T\langle\sigma_{\rm sec}(\Delta\Omega)\rangle_{\rm av}\mathfrak{N}_A}{A}.$$

Since, by definition, $\sigma_{\rm geom}R(E_\pi)=\sigma_{\rm abs}$, that is, $\lambda_{\rm geom}=\lambda_{\rm abs}R(E_\pi)$, we can finally rewrite Eq. (B5) as follows:

$$N_{\rm tot}=N_{\rm tot,pr}+N_{\rm tot,sec}$$
$$=\left[N_0\exp\left(-\sum_{i=1}^{n}\frac{x_i}{\lambda_{i,\rm geom}}\langle R(E_{\pi,i})\rangle_{\rm av}\right)\right]F_C, \tag{B9}$$

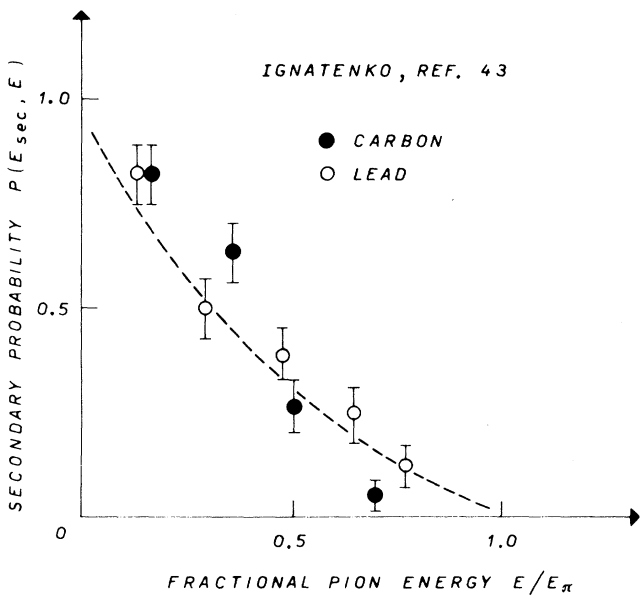

FIG. 28. The probability, $P(E_{\rm sec}>E)$, that the energy of a secondary, E_s (produced by a primary pion of energy E_π) is greater than E, as a function of the fractional energy E/E_π.

with

$$F_C=1+\sum_{i=1}^{n}\frac{x_i\langle\sigma_{i,\rm sec}(\Delta\Omega)\rangle_{\rm av}\mathfrak{N}_A}{A}.$$

Notice that F_C is a correction factor multiplying the normal absorption term [Eq. (B2)] $N_{\rm tot,pr}$.

3. Calculation of Corrections

We will now calculate the absorption and secondary-particle production corrections for a pion entering normally the series of absorbers constituting our telescopes ($\psi=0$, i.e., in the above expression [Eq. (B9)] $x_i=t_i$).

From the list of materials given in Table VIII we can first calculate the absorption corrections $N_{\rm tot,pr}$, i.e., the first terms of Eq. (B9). This calculation gives for each of the counter systems we are interested in [i.e., trigger counters $=AB(C+D)$; mark counters $=AB(C+D)(CR_1+CR_2)$; anticoincidence counters $=AB(C+D)(CR_3+CR_4)$]:

$$N_{\rm tot,pr}(\text{trigger})=\left[N_0\exp\left(-\sum_{i=1}^{n}\frac{x_i}{\lambda_{i,\rm geom}}R(E_\pi)\right)\right]$$
$$=N_0e^{-0.27R(E_\pi)},$$
$$N_{\rm tot,pr}(\text{mark})=N_0e^{-2.1R(E_\pi)},$$
$$N_{\rm tot,pr}(\text{anticoincidence})=N_0e^{-2.67R(E_\pi)}.$$

As an example, for 400-MeV pions the fraction of remaining particles at each final counter plane is:

trigger counters = 82%.

mark counters = 21%,

anticoincidence counters = 15%.

To evaluate the effect of secondary corrections we must in addition use the average solid angle of each final counter as seen by each absorber and the range cut on the produced secondaries of each absorber. The values of F_C [second term in Eq. (B9)] for several incident pion energies are listed in Table IX. As can be seen from Eq. (B9), when the primary pion energy is such that F_C is equal to

TABLE IX. The values of F_C (secondary-particle production correction) are listed at several pion kinetic energies for the three counter systems of interest.

Pion kinetic energy E_π (MeV)	F_C Trigger counters	Mark counters	Anticoincidence counters
400	1.047	1.000	
500	1.099	1.098	
600	1.150	1.588	1.133
1000	1.413	5.159	3.24
1500	1.573	10.61	8.389

$$\exp\left(+\sum_{i=1}^{n}\frac{x_i}{\lambda_{i,\mathrm{geom}}}\langle R(E_\pi)\rangle_{\mathrm{av}}\right),$$

all the absorbed pions have produced a secondary that reached the final counter. Clearly for energies higher than this balanced absorption energy there is not a correction for pion absorption. For each counter system of our apparatus this balanced absorption energy point is:

trigger counters $\simeq 800$ MeV,

mark counters $\simeq 1000$ MeV,

anticoincidence counters $\simeq 1500$ MeV.

All of the values listed in Table IX refer to secondary-particle production corrections for a single pion.

The effects of all these absorption and secondary-particle production corrections on the values of the detection efficiencies for various produced final states are discussed in Appendix A.

---

[1]J. E. Augustin, J. C. Bizot, J. Buon, J. Haissinski, D. Lalanne, P. Marin, J. Perez-y-Jorba, F. Rumpf, E. Silva, and S. Tavernier, Phys. Rev. Letters 20, 126 (1968); J. E. Augustin, D. Benaksas, J. Buon, F. Fulda, V. Gracco, J. Haissinski, D. Lalanne, F. La Planche, J. Lefrancois, P. Lehmann, P. Marin, J. Perez-y-Jorba, F. Rumpf, and E. Silva, Lett. Nuovo Cimento 2, 214 (1969); J. C. Bizot, B. Delcourt, J. Jeanjean, D. Lalanne, J. Perez-y-Jorba, F. Richard, F. Rumpf, and D. Triell, *ibid.* 4, 1273 (1970).

[2]U. L. Auslander, G. I. Budker, Ju. N. Pestov, V. A. Sidorov, A. N. Skrinsky, and A. G. Khabakhpashev, Phys. Letters 25B, 433 (1967); V. E. Balakin, G. I. Budker, E. V. Pakhtosova, V. A. Sidorov, A. N. Skrinsky, G. M. Tumaikin, and A. G. Khabakhashev, *ibid.* 34B, 328 (1971).

[3]Boson Group: B. Bartoli, B. Coluzzi, F. Felicetti, G. Goggi, G. Marini, F. Massa, D. Scannicchio, V. Silvestrini, and F. Vanoli, Nuovo Cimento 70A, 603 (1970); 70A, 615 (1970).

[4]Boson Group: B. Bartoli, F. Felicetti, G. Marini, A. Nigro, H. Ogren, N. Spinelli, V. Silvestrini, and G. Vanoli, Phys. Letters 36B, 593 (1971); 36B, 598 (1971).

[5]Frascati-Roma-Padova-Maryland Collaboration ($\mu\pi$ Group): B. Borgia, M. Conversi, M. Grilli, E. Iarocci, M. Nigro, L. Paoluzi, P. Spillantini, L. Trasatti, V. Valente, R. Visentin, and G. T. Zorn, in *Proceedings of the International Symposium on Electron and Photon Interactions at High Energies, 1971,* edited by N. B. Mistry (Cornell Univ. Press, Ithaca, N. Y., 1972).

[6]$\gamma\gamma$ Group: C. Bacci, R. Baldini-Celio, G. Capon, C. Mencuccini, G. P. Murtas, G. Penso, A. Reale, G. Salvini, M. Spinetti, and B. Stella, in *Proceedings of the International Symposium on Electron and Photon Interactions at High Energies, 1971,* edited by N. B. Mistry (Cornell Univ. Press, Ithaca, N. Y., 1972).

[7]Among others: S. Ferrara, M. Greco, and A. F. Grillo, Lett. Nuovo Cimento 4, 1 (1970); N. Cabibbo, G. Parisi, and M. Testa, *ibid.* 4, 34 (1970); J. D. Bjorken and S. J. Brodsky, Phys. Rev. D 1, 1416 (1970); G. Kramer, J. L. Uretsky, and T. F. Walsh, *ibid.* 3, 719 (1971); J. Layssac and F. M. Renard, Lett. Nuovo Cimento 1, 197 (1971); M. T. Vaughn and P. J. Polito, *ibid.* 1, 74 (1971); A. Bramòn and M. Greco, *ibid.* 1, 739 (1971); Frascati Reports No. LNF-71/8, 1971 and No. LNF-71/97, 1971 (unpublished).

[8]E. D. Bloom, D. H. Coward, H. DeStaebler, J. Drees, G. Miller, L. W. Mo, R. E. Taylor, M. Breidenbach, J. I. Friedman, G. H. Hartmann, and H. W. Kendall, Phys. Rev. Letters 23, 930 (1969); M. Breidenbach, J. I. Friedman, H. W. Kendall, E. D. Bloom, D. H. Coward, H. DeStaebler, J. Drees, L. W. Mo, and R. E. Taylor, *ibid.* 23, 935 (1969).

[9]The source of our events (which is defined as the region of interaction of positron and electron bunches) has a finite-energy-dependent length. In fact, it is expected to have a longitudinal distribution

$$N(l_z)=N_0\exp(-l_z^2/2\bar{l}_z^2),$$

where $\bar{l}_z$ (cm) is theoretically expected to be $20\times E^{3/2}$ ($E_\pm$ GeV) and experimentally has been determined as $(22\pm2)E^{3/2}$ (private communication of the Adone machine staff). This reduces the effective solid angle of the apparatus by a factor of the order of 2.

[10]In each chamber, the magnetostrictive pickup coil was placed at the edge which is nearer to the horizontal plane, i.e., at $\varphi=28°$ and 332° for chambers 1 and 4, and at $\varphi=152°$ and 208° for chambers 2 and 3.

[11]In Adone there are three bunches of e^- and three bunches of e^+, each of duration 1–2 nsec (FWHM). They cross the rf cavity when the phase has a fixed value Φ (synchronous phase, slightly dependent on the machine energy), and collide in the experimental sections every ~ 117 nsec. The beam-beam impact occurs thus at a fixed time with respect to the time when the rf phase assumes its synchronous value Φ.

[12]We recall that the luminosity L of a storage ring at one of the interaction regions for head-on collisions of two beams uniformly distributed into k bunches per beam, with overlapping transverse Gaussian distributions whose rms dimensions $\bar{l}_x$, $\bar{l}_y$ are equal, is given by

$$L=\frac{1}{kf_0e^2}\frac{I_{e^+}I_{e^-}}{4\pi\bar{l}_x\bar{l}_y},$$

where I_{e^+} and I_{e^-} are the positron and electron beam currents, f_0 is the revolution frequency of the beams, and e is the electron charge. L provides a measurement of the machine intensity, in the sense that the rate $\dot{n}$ of events produced at one crossing region from a process of cross section σ is given by $\dot{n}=L\sigma$.

[13]G. Barbiellini, B. Borgia, M. Conversi, and R. Santonico, Rend. Classe Sci. Mat. Fis. Nat. Accad. Naz. Lincei 44, 233 (1968); H. C. Dehne and M. Preger, Frascati Report No. LNF-70/33, 1970 (unpublished).

[14]It is worthwhile to note that an independent check of luminosity performed by the machine group measuring the γ rays emitted at forward angles from e^+e^- single and

double bremsstrahlung reactions agrees, to within ~ 10%, with the Bhabha monitor luminosity data.

[15]By definition, $\Delta\varphi$ is zero when the two particles go in opposite directions. Particularly for the multiparticle analysis, we have found it convenient to define the sign of $\Delta\varphi$ in a specular way for left and right telescopes; i.e., if we consider the two half-planes defined by the azimuthal projection of the particle trajectory which goes in a top telescope (T_1 or T_2), $\Delta\varphi$ will be positive if the second particle lies in the half-plane containing the other top telescope. (In the multiparticle case, if both particles go in the bottom telescopes $\Delta\varphi$ is consistently defined as positive).

[16]The inefficiencies of our monogap spark chambers, which are essentially due to impurity in the Ne-He gas and malfunctioning of the trigger spark gaps, are variable in time and differ for the various chambers. The values, of the efficiencies averaged on the whole period, turned out to be: $\epsilon_{\alpha_1}=0.86$, $\epsilon_{\beta_1}=0.71$, $\epsilon_{\alpha_2}=0.86$, $\epsilon_{\beta_2}=0.85$, $\epsilon_{\alpha_3}=0.84$, $\epsilon_{\alpha_4}=0.89$, $\epsilon_{\beta_4}=0.93$. They have been experimentally determined from the analysis of the e^+e^- scattering events in which only one chamber had not fired. In addition, from the e^+e^- elastic scattering events we have determined that the effect of spurious tracks in the chambers was completely negligible.

[17]Y. S. Tsai, in *Proceedings of the International Symposium on Electron and Photon Interactions at High Energies, Hamburg, 1965* (Springer, Berlin, 1965), p. 380; Phys. Rev. 120, 269 (1960); V. N. Bayer and S. A. Kheifets, Nucl. Phys. 47, 313 (1963).

[18]S. Tavernier, Ph.D. thesis, Orsay Internal Report No. 68/7, 1968 (unpublished).

[19]A. Rich, Phys. Rev. Letters 20, 967 (1968).

[20]As was described in Sec. III, the monitor apparatus is operated in a contiguous straight section of Adone. Due to the symmetry of the machine and the fact that the data were collected during a long period of time (averaging over slight variations in the working conditions), it is reasonable to assume that the over-all results are unaffected by the fact that small- and large-angle elastic scattering were measured in different straight sections of Adone.

[21]M. Curatolo, Ph.D. thesis, University of Rome (unpublished).

[22]If one wants to express the experimental result in terms of a cutoff parameter Λ, using an amplitude modification $(1 \pm q^2/\Lambda_\pm^2)^{-1}$, from the quoted errors one obtains (at a 95% confidence level) $\Lambda_+ = 3.9$ GeV/c, $\Lambda_- = 5.4$ GeV/c. The q^2 value used [$q^2 = 1.52$ (GeV/c)^2] corresponds to the center of the energy range explored.

[23]For example: Two particles entering the two top (bottom) telescopes T_1, T_2 (T_3, T_4) will have, by definition, positive $\Delta\varphi$, while the $\Delta\varphi$ corresponding to particles entering vertical pair of telescopes (T_1, T_4 or T_2, T_3) will have negative sign.

[24]V. N. Baier and V. S. Fadin, Phys. Letters 53B, 156 (1971).

[25]The theoretical $\Delta\varphi$ distribution for the $e^+e^- \to e^+e^-\pi^+\pi^-$ reaction is quite similar to the distribution for $e^+e^- \to e^+e^-e^+e^-$ shown in Fig. 15(a). See S. J. Brodsky, J. Kinoshita, and H. Terazawa, Phys. Rev. D 4, 1532 (1971).

[26]The Monte Carlo program is the same one we have used to compute the detection efficiency of noncoplanar events. The electrons were generated according to the QED scattering cross section. Spark-chamber efficiencies and effects of the extended source (see Ref. 9, Sec. II) were taken into account, as well as all the geometrical features of the apparatus (cf. also Appendix A).

[27]The spark efficiency of the monogap spark chambers depends on (among other things) the angle ψ between the direction of the particle which crosses the chamber and the normal to the chamber plates. Due to the finite longitudinal dimension of the source which is comparable to the linear dimensions of our apparatus (see Ref. 9, Sec. II), the ψ distribution of the particles associated with noncoplanar events is broader than the corresponding Bhabha electrons ψ distribution. Consequently, the noncoplanar particles are detected by our spark chambers with efficiencies $\epsilon_{n.c.}$ which are lower than the spark efficiencies for Bhabha electrons ϵ_e (listed in Ref. 9), by a factor which has been experimentally determined to be $\gamma = \epsilon_{n.c.}/\epsilon_e = 0.95 \pm 0.01$.

[28]A. Bramòn and M. T. Greco, Lett. Nuovo Cimento 3, 693 (1972).

[29]J. Layssac and F. M. Renard, Lett. Nuovo Cimento 1, 197 (1971); Nuovo Cimento 6A, 134 (1971).

[30]M. T. Vaughn and P. J. Polito, Lett. Nuovo Cimento 1, 74 (1971).

[31]M. Davier, I. Derado, D. C. Fries, F. F. Liu, R. Z. Mozley, A. C. Odian, J. Park, W. P. Swanson, F. Villa, and D. Yount, SLAC report, 1971 (unpublished); paper presented at the International Symposium on Electron and Photon Interactions at High Energy, Cornell, 1971 (unpublished).

[32]At 1.82 and 2.30 GeV c.m. energies we rejected solutions with $P(\chi^2) \leq 50\%$. At. 1.51 GeV we had to adopt a different $P(\chi^2)$ cut. This is due to the fact that the fraction, f_M, of marked events is experimentally $(15 \pm 5)\%$, which is about 2 standard deviations above the predictions of any possible fit. This contributes about 4 to the χ^2 of all the possible solutions. After having tested that a 1 standard deviation downwards shift of f_M would reproduce at 1.51 GeV the same χ^2 behavior we found at the other energies, and that the cross-section values would be unaffected, we have lowered this $P(\chi^2)$ cut to 5%.

[33]F. Cerulus, Suppl. Nuovo Cimento 15, 402 (1960).

[34]For example, the experimental determination of the ratio $x = \sigma_{2\pi^\pm, N}/\sigma_{\geq 4\pi^\pm, \text{tot}}$ by the other Adone groups can be seen directly from Figs. 23(b) and 23(c).

[35]ACO results: J. Lefrancois, invited talk on the Orsay results at the International Symposium on Electron and Photon Interactions at High Energy, Cornell, 1971 (unpublished).

[36]Novosibirsk results: V. A. Sidorov, invited talk on the Novosibirsk results at the International Symposium on Electron and Photon Interactions at High Energy, Cornell, 1971 (unpublished).

[37]Adone $\gamma\gamma$ Group results: C. Bacci, R. Baldini-Celio, G. Capon, C. Mencuccini, G. P. Murtas, G. Penso, A. Reale, G. Salvini, M. Spinetti, and B. Stella, Phys. Letters 38B, 551 (1972).

[38]Adone $\mu\pi$ Group results: G. Barbarino, F. Ceradini, M. Conversi, M. Grilli, E. Iarocci, M. Nigro, L. Paoluzi, R. Santonico, P. Spillantini, L. Trasatti, V. Valente, R. Visentin, and G. T. Zorn, Lett. Nuovo Cimento 3, 689 (1972); see also M. Grilli, Frascati Report No. LNF-71/100, 1971 (unpublished).

[39]J. C. Caris, E. A. Knapp, V. Perez-Mendez, and W. A. Perkins, Phys. Rev. 126, 295 (1962).

[40]J. W. Cronin, R. Cool, and A. Abashian, Phys. Rev. 107, 1121 (1957).
[41]R. L. Martin, Phys. Rev. 87, 1052 (1954).
[42]M. J. Longo and B. J. Moyer, Phys. Rev. 125, 701 (1962).
[43]A. E. Ignatenko, in *Proceedings of the CERN Symposium on High-Energy Accelerators and Pion Physics, Geneva, 1956* (European Organization of Nuclear Research, Geneva, 1956), Vol. 2, p. 313.

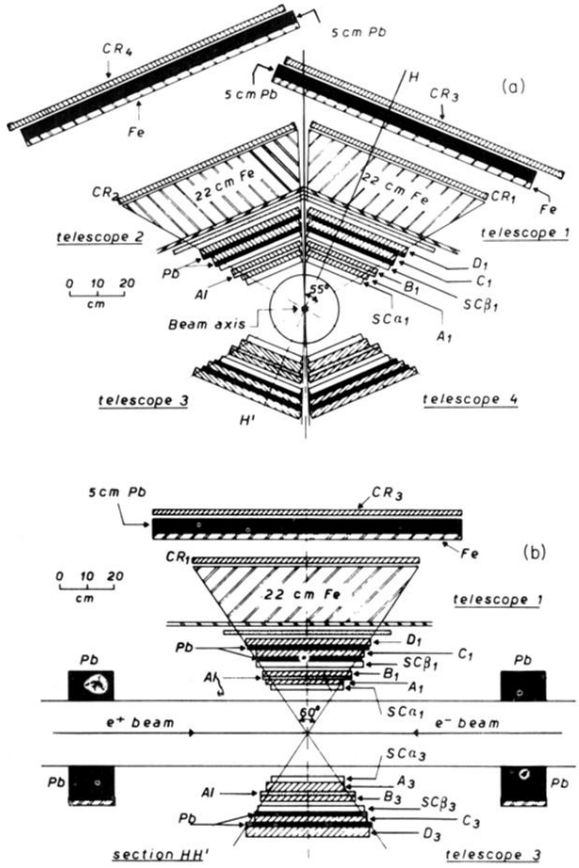

FIG. 1. The experimental apparatus. (a) Section orthogonal to the beam axis: A_i, B_i, C_i, D_i are plastic scintillator counters; $SC\alpha_i$ and $SC\beta_i$ are magnetostrictive monogap wire chambers; CR_i's are veto counters for cosmic rays. (b) Section (along H, H') in a plane through the beam direction and orthogonal to a pair of opposite telescopes.